Inverse modeling of pan-Arctic methane emissions at high spatial resolution: What can we learn from assimilating satellite retrievals and using different process-based wetland and lake biogeochemical models?

Zeli Tan[1,2], Qianlai Zhuang[1,2,3], Daven K. Henze[4], Christian Frankenberg[5], Ed Dlugokencky[6], Colm Sweeney[6], Alexander J. Turner[7], Motoki Sasakawa[8], Toshinobu Machida[8]

[1]Department of Earth, Atmospheric, and Planetary Sciences, Purdue University, West Lafayette, Indiana, USA

[2]Purdue Climate Change Research Center, Purdue University, West Lafayette, Indiana, USA

[3]Department of Agronomy, Purdue University, West Lafayette, Indiana, USA

[4]Department of Mechanical Engineering, University of Colorado, Boulder, Colorado, USA

[5]Jet Propulsion Laboratory/California Institute of Technology, Pasadena, California, USA

[6]Global Monitoring Division, NOAA Earth System Research Laboratory, Boulder, Colorado, USA

[7]School of Engineering and Applied Sciences, Harvard University, Cambridge, Massachusetts, USA

[8]National Institute for Environmental Studies, Tsukuba, Japan

Correspondence to: Qianlai Zhuang (qzhuang@purdue.edu)

Abstract: Understanding methane emissions from the Arctic, a fast warming carbon reservoir, is important for projecting future changes in the global methane cycle. Here we optimized methane emissions from north of 60°N (pan-Arctic) regions using a nested-grid high-resolution inverse model that assimilates both high-precision surface measurements and column-average SCIAMACHY satellite retrievals of methane mole fraction. For the first time, methane emissions from lakes were integrated into an atmospheric transport and inversion estimate, together with prior wetland emissions estimated with six biogeochemical models. In our estimates, in 2005, global methane emissions were in the range of 496.4–511.5 Tg yr^{-1} and pan-Arctic methane emissions were in the range of 11.9–28.5 Tg yr^{-1}. Methane emissions from pan-Arctic wetlands and lakes were 5.5–14.2 Tg yr^{-1} and 2.4–14.2 Tg yr^{-1}, respectively. Methane emissions from Siberian wetlands and lakes are the largest and also have the largest uncertainty. Our results indicate that the uncertainty introduced by different wetland models could be much larger than the uncertainty of each inversion. We also show that assimilating satellite retrievals can reduce the uncertainty of the nested-grid inversions. The significance of lake emissions cannot be identified across the pan-Arctic by high-resolution inversions but it is possible to identify high lake emissions from some specific regions. In contrast to global inversions, high-resolution nested-grid inversions perform better in estimating near surface methane concentrations.

1. Introduction

Methane (CH_4) is the second most powerful carbon-based greenhouse gas in the atmosphere behind carbon dioxide (CO_2) and also plays a significant role in the cycles of ozone, hydroxyl radicals (OH) and stratospheric water vapor (Myhre et al., 2013; Shindell et al., 2009). The atmospheric burden of CH_4 is now more than factor of 2.5 greater than the pre-industrial value of about 700 ppb (Etheridge et al., 1998), mainly due to anthropogenic emissions. Major sources and sinks of CH_4 have been identified (Denman et al., 2007); however their quantification is still of large uncertainties and the annual and inter-annual variability of atmospheric CH_4 are not well explained. For instance, scientists have not yet agreed on what caused the leveling off of atmospheric CH_4 since the 1980s (Dlugokencky et al., 2003; Bousquet et al., 2006; Aydin et al., 2011; Kai et al., 2011; Levin et al., 2012; Simpson et al., 2012; Kirschke et al., 2013) and the recent rebounding of its growth since 2007 (Rigby et al., 2008; Dlugokencky et al., 2009; Nisbet et al., 2014).

To reduce the quantification uncertainty of CH_4 sources and sinks, much effort has been made using Bayesian inference (Bergamaschi et al., 2007, 2009, 2013; Meirink et al., 2008; Cressot et al., 2014; Houweling et al., 2014; Alexe et al., 2015). In these studies, in-situ and/or satellite observations of CH_4 that are representative of large spatial scales were assimilated into a chemical transport model (CTM) to constrain the initial estimates of CH_4 sources and sinks that are inventoried from field studies, industrial investigations and biogeochemical models (Fung et al., 1991; Zhuang et al., 2004; Walter et al., 2006; Zhu et al., 2013; Tan and Zhuang, 2015a and 2015b). Space-borne observations of atmospheric CH_4 are especially useful in inverse modeling because they can deliver dense and continuous coverage unachievable by surface networks or aircraft campaigns (Bergamaschi et al., 2007). There are two types of nadir satellite CH_4

retrievals: one from solar backscatter in the shortwave infrared (SWIR) and the other from thermal infrared radiation (TIR). Between them, SWIR retrievals were more widely used in atmospheric inversion of CH_4 emissions (Bergamaschi et al., 2007, 2009, 2013; Fraser et al., 2013; Cressot et al., 2014; Houweling et al., 2014; Monteil et al., 2014; Wecht et al., 2014; Alexe et al., 2015; Turner et al., 2015) because they can provide column concentrations with near-uniform vertical sensitivity down to the surface. To date, most of the inversions were operated at coarse spatial resolutions over 300 km. However, partly owing to their coarse resolutions, it is impossible for these inversions to constrain different CH_4 sources that are spatially co-located (Fung et al., 1991; Wecht et al., 2014). To address this issue, regional inverse models at fine spatial resolutions were developed (Miller et al., 2013; Wecht et al., 2014; Thompson et al., 2015). For example, Wecht et al. (2014) and Turner et al. (2015) have used the 1/2° × 2/3° horizontal resolution GEOS-Chem adjoint model to constrain CH_4 emissions over North America.

Estimating CH_4 emissions from the Arctic is important for understanding the global carbon cycle because the fast warming of Arctic permafrost, one of the largest organic carbon reservoirs (Tarnocai et al., 2009), could lead to a rapid rise of CH_4 emissions (Zhuang et al., 2006; Walter et al., 2007; Koven et al., 2011). Natural sources dominate the Arctic CH_4 inventory (Fisher et al., 2011), e.g. wetlands (McGuire et al., 2012), lakes (Walter et al., 2006; Bastviken et al., 2011), sea shelves (Berchet et al., 2016; Myhre et al., 2016) and oceans (Kort et al., 2012). As the factors governing natural CH_4 production (methanogenesis) and oxidation (methanotrophy) are notoriously heterogeneous, estimates of Arctic CH_4 emissions are still poorly constrained, even with decades of site-level and modeling studies (Zhuang et al., 2004; Bastviken et al., 2011; Schuur et al., 2015; Tan and Zhuang, 2015a; Tan and Zhuang, 2015b).

Previous CH_4 inversions over the Arctic only assimilated surface measurements that were too sparse to constrain fine-scale CH_4 fluxes. Also, possibly important CH_4 sources that were newly identified, e.g. CH_4 emissions from Arctic lakes (Walter et al., 2006 and 2007; Bastviken et al., 2011; Tan and Zhuang, 2015a) and the East Siberian Shelf (Berchet et al., 2016; Thornton et al., 2016) have not been included in these studies. Given the ill-posed nature of trace-gas inversions, realistic prior fluxes could be important for successful inverse modeling of CH_4 emissions from the Arctic (Kaminski and Heimann, 2001).

To address these issues, we used the adjoint of a 3-D CTM at a high spatial resolution (less than 60 km) to improve the quantification of pan-Arctic CH_4 emissions in 2005. We explored the feasibility of using satellite CH_4 retrievals overpassing the pan-Arctic to further constrain regional CH_4 emissions. For the first time, CH_4 emissions from pan-Arctic lakes were included in high-resolution inverse modeling of CH_4 emissions. As wetland emissions are likely the largest pan-Arctic CH_4 source, we also investigated the sensitivity of our estimates to the use of different wetland emission scenarios. Section 2 describes the observation data of atmospheric CH_4 that were used to infer CH_4 emissions and evaluate posterior estimates. Section 3 details the wetland and lake biogeochemical models that were used in this study (Section 3.1), the pan-Arctic nested-grid CTM (Section 3.2), and the adjoint-based inversion method (Section 3.3). Section 4 presents the posterior CH_4 emissions, their evaluation and further discussion.

2. Observations

2.1. Satellite Retrievals

SWIR CH_4 retrievals are available from SCanning Imaging Absorption spectroMeter for Atmospheric CHartogrphY (SCAMACHY) for 2003–2012 (Frankenberg et al., 2006, 2008, 2011)

and Greenhouse Gases Observing SATellite (GOSAT) for 2009 to present (Parker et al., 2011). SCIAMACHY, aboard the European Space Agency's environmental research satellite ENVISAT retrieves column-averaged CH_4 mixing ratios (XCH_4) from the SWIR nadir spectra (channel 6: 1.66–1.67 μm) using the IMAP-DOAS algorithm (Frankenberg et al., 2006, 2008, 2011). The satellite operates in a near polar, sun-synchronous orbit at an altitude of 800 km. At channel 6, the ground pixel size of the retrievals is about 30 km (along-track) × 60 km (across-track). We use version 6.0 proxy CH_4 retrievals from Frankenberg et al. (2011) that provide a weighted column average dry-mole fraction of CH_4 with 10-layer averaging kernels and prior CH_4 profiles. The averaging kernels show near-uniform vertical sensitivity in the troposphere and declining sensitivity above the tropopause (Butz et al., 2010). Some auxiliary data, e.g. the air mass factor A_F ($A_F = 1/\cos\theta + 1/\cos\xi$, where θ is the solar zenith angle and ξ is the viewing angle of the satellite), water column density and dry air column density, are also published with the IMAP-DOAS v6.0 XCH_4 product.

The estimated single-retrieval precision is scene-dependent and averages roughly 1.5% or 25 ppb (Frankenberg et al., 2011). With this order of instrument precision, SCIAMACHY cannot resolve day-to-day variability of emissions but can strongly constrain a multi-year average (Turner et al., 2015). The retrieving algorithm firstly calculates CH_4 total column density Ω_{CH4} (molecules cm^{-2}):

$$\Omega_{CH_4} = \Omega_{\mathbf{A}} + \mathbf{a}^{\mathrm{T}}\left(\omega - \omega_{\mathbf{A}}\right) \qquad (1)$$

where ω is the true 10-layer sub-column densities of CH_4 (molecules cm^{-2}), $\omega_{\mathbf{A}}$ is the 10-layer prior CH_4 sub-column density (molecules cm^{-2}), $\Omega_{\mathbf{A}}$ is the corresponding a priori CH_4 total column density, and **a** is an averaging kernel vector that defines the sensitivity of the retrieved total column to each sub-column in ω. To account for the impact of aerosol scattering and

instrument effects on the observed light path, Frankenberg et al. (2006) used the CO_2 column density Ω_{CO2} as a proxy to normalize and convert Ω_{CH4} to a column mixing ratio XCH_4 (ppb):

$$XCH_4 = \left(\Omega_{CH_4} / \Omega_{CO_2}\right) XCO_2 \qquad (2)$$

where XCO_2 is the column-weighted mixing ratio of CO_2 from NOAA's CarbonTracker CO_2 measurement and modeling system. CO_2 is used as a proxy because it is retrieved in a spectrally neighboring fitting window and, relative to CH_4, its mixing ratio is known with much higher precision.

The quality of SCIAMACHY observations is controlled by a filtering scheme that selects only daytime, over land and with cloud free or partially cloud scenes and good fitting accuracy (http://www.temis.nl/climate/docs/TEMIS_SCIA_CH4_IMAPv60_PSD_v2_6.pdf). Further, a surface elevation filter is applied to filter out observations that are different from the model grids at surface altitude by more than 250 m (Bergamaschi et al., 2009; Alexe et al., 2015). This filtering process ensures that the atmospheric columns seen by SCIAMACHY are well represented by the model columns. To avoid spurious outliers that may have a large impact on the inversion, XCH_4 retrievals of less than 1500 ppb or larger than 2500 ppb are discarded (Alexe et al., 2015). For the pan-Arctic, most of qualified XCH_4 retrievals were recorded in the summer time when local solar zenith angles are higher, surface reflectance is lower and impact of Arctic vortex is smaller. Fig. 1 shows the SCIAMACHY retrievals (n = 37743) of the weighted column-average CH_4 dry mixing ratio for July 2005–September 2005 in the pan-Arctic that have passed all quality control tests.

2.2. Surface Observations

The NOAA/ESRL Carbon Cycle Cooperative Global Air Sampling Network provides high-precision weekly flask measurements of surface atmospheric CH_4 dry-air mole fraction (Dlugokencky et al., 2014) that were calibrated against the WMO X2004 CH_4 standard scale maintained at NOAA (Dlugokencky et al., 2005). Due to the coarse resolution of the GEOS-Chem model, we include only marine and continental background sites and exclude sites that are strongly influenced by sub-grid local sources (Alexe et al., 2015), as listed in Table S1. The flask-air samples in the NOAA/ESRL network that were taken from regular ship cruises in Pacific Ocean serve to evaluate simulated surface mixing ratios of global inversions over the remote ocean and downwind the continental sources (Alexe et al., 2015). Fig. 1 shows the Arctic sites that were used for data assimilation and nested-grid inversion evaluation.

2.3. Aircraft Campaign Observations

To derive the bias of SCIAMACHY CH_4 retrievals overpassing the pan-Arctic and evaluate the modeled CH_4 vertical profiles in the troposphere, we used CH_4 measurements that were collected by three aircraft campaigns: the NOAA/ESRL Carbon Cycle Cooperative Global Air Sampling Network's aircraft program (http://www.esrl.noaa.gov/gmd/ccgg/aircraft/data.html; Sweeney et al., 2015), the National Institute for Environmental Studies (NIES) aircraft program (Machida et al., 2001; Sasakawa et al., 2013), and the NASA's Arctic Research of the Composition of the Troposphere from Aircraft and Satellite (ARCTAS) mission. For the NOAA/ESRL aircraft mission, CH_4 was routinely collected using 0.7 L silicate glass flasks on planned flights with maximum altitude limits of 300–350 hPa. The sampling vertical resolution is up to 400 m in the boundary layer and all samples were analyzed by NOAA/ESRL in Boulder, Colorado. For the NIES aircraft mission, air samples were collected in 550 mL glass flasks over Surgut, West Siberia (61.5°N, 73.0°E) at altitude ranging from 0.5 to 7 km with 0.5–1.5 km

intervals. The precision of gas chromatograph analysis for CH_4 measurement was estimated to be 1.7 ppb and the NIES-94 scale used in analysis was higher than the NOAA/GMD scale by 3.5–4.6 ppb in a range of 1750–1840 ppb. In ARCTAS, CH_4 was measured over northern Canada by the DACOM tunable diode laser instrument with an estimated accuracy/precision of 1%/0.1%. Central locations of their flights in the pan-Arctic are shown in Fig. 1. Table S2 lists the locations and profiles of the NOAA/ESRL aircraft mission flights used in evaluation.

3. Modeling

Here we describe the prior emissions, the forward model, and the inversion method used to optimize CH_4 emissions in the pan-Arctic on the basis of SCIAMACHY and NOAA/ESRL observations.

3.1. Wetland and Lake CH_4 Emissions

CH_4 emissions estimated by the inverse modeling method can be sensitive to the choice of prior wetland CH_4 fluxes (Bergamaschi, 2007). To assess this sensitivity, we used wetland CH_4 emissions simulated by six well-known wetland biogeochemical models (CLM4Me, DLEM, LPJ-Bern, LPJ-WSL, ORCHIDEE and SDGVM) to setup six different inverse modeling experiments. All wetland CH_4 simulations follow the same protocol of WETland and Wetland CH_4 Inter-comparison of Models Project (WETCHIMP) as described in Melton et al. (2013) and Wania et al. (2013). Melton et al. (2013) demonstrated that the difference of these estimates primarily arises from the model distinction in CH_4 biogeochemistry and wetland hydrology. These models estimated that the annual global CH_4 emissions from wetlands during 2004–2005 were in the range of 121.7–278.1 Tg yr^{-1} (Fig. S1) and wetland CH_4 emissions are the highest in tropical regions (e.g., Amazon, Southeast Asia and Tropical Africa) where extensive floodplains

and warm environment coexist. In the pan-Arctic, the modeled annual wetland CH_4 emissions in 2005 were in the range of 9.1–20.9 Tg yr^{-1} (Fig. 2), and their spatial distribution was mainly controlled by the modeled or mapped wetland coverage (Melton et al., 2013). As shown in Fig. 2, because of some consistency in simulating wetland hydrology, nearly all models suggest that there are high CH_4 fluxes in West Siberia Lowlands, Finland and Canadian Shield.

Lakes, permanent still-water bodies without direct connection to the sea, are abundant in the pan-Arctic (Lehner and Döll, 2004). Recent studies indicated that pan-Arctic lakes could contribute a significant amount of CH_4 to the atmosphere (Walter et al., 2006; Tan and Zhuang, 2015a) and the emissions could be driven by factors different from wetland emissions, e.g. the supply of labile yedoma permafrost carbon (Walter et al., 2006) and water deep mixing (Schubert et al., 2012). Because the WETCHIMP models cannot account for this source, we used a one-dimension process-based lake biogeochemical model, bLake4Me, to simulate CH_4 emissions from pan-Arctic lakes (Tan et al., 2015; Tan and Zhuang, 2015a). The bLake4Me model explicitly parameterizes the control of temperature and carbon substrate availability on methanogenesis, the control of temperature and oxygen level on methanotrophy and the transport of gaseous CH_4 by diffusion and ebullition. A detailed model description and evaluation can be found in Tan et al. (2015). Model quantification of CH_4 emissions from all lakes north of 60°N was described by Tan and Zhuang (2015a and 2015b). On average, the estimated CH_4 emissions from pan-Arctic lakes during the studied period are approximately 11 Tg CH_4 yr^{-1}, see Fig. 2.

3.2. GEOS-Chem Model

Atmospheric CH_4 mole fractions are simulated by GEOS-Chem v9-01-03 (http://acmg.seas.harvard.edu/geos/index.html), a global 3-D CTM model (Bey et al., 2001). For

the period of 2004–2005, GEOS-Chem is driven by GEOS-5 meteorological (hereafter GEOS-5 met) data from NASA's Global Modeling Assimilation Office (GMAO). The GEOS-5 met data have horizontal resolution of 1/2° latitude × 2/3° longitude, temporal resolution of 6 hours and 72 hybrid sigma-pressure levels extending from Earth's surface to 0.01 hPa. In contrast to the global GEOS-Chem model, the nested-grid version does not include algorithms for handling advection near the North and South Poles (Lin and Rood, 1996). To avoid polar grid boxes, we crop the native 1/2° × 2/3° resolution GEOS-5 met data to a window region (180°W–180°E and 80°N–56°N) for the pan-Arctic nested grid. To make it consistent with the bLake4Me model, only CH_4 emissions north of 60°N are analyzed. We expect that the avoidance of the North Pole only has a minor impact on our inversions because according to Miyazaki et al. (2008) the Northern Hemisphere (NH) extratropics during summer has slow mean-meridional circulation and inactive wave activity but strong vertical transport. Boundary conditions for nested grid simulations are produced using the same period GEOS-Chem 4° × 5° resolution global scale forward runs at 3-hour intervals.

The GEOS-Chem CH_4 simulation was originally introduced by Wang et al. (2004) and updated by Pickett-Heaps et al. (2011). As described by Wecht et al. (2014), the prior anthropogenic sources, including oil/gas production, coal mining, livestock, waste treatment, rice paddies, biofuel burning and other processes, were extracted from Emission Database for Global Atmospheric Research v4.2 (EDGAR4.2) with 0.1° × 0.1° resolution and no seasonality (European Commission, Joint Research Centre/Netherlands Environmental Assessment Agency, 2009). CH_4 emissions from termites and biomass burning were obtained from the study of Fung et al. (1991) and daily Global Fire Emissions Database Version 3 (GFED3) of van der Werf et al. (2010), respectively. CH_4 emissions from wetlands and lakes were simulated by biogeochemical

models described in Section 3.1. Atmospheric CH_4 is mainly removed by tropospheric oxidation initiated by reaction with tropospheric OH, which was computed using a 3-D OH climatology of monthly average concentrations from a previous simulation of tropospheric chemistry (Park et al., 2004). The global mean pressure-weighted tropospheric OH concentration is 10.8×10^5 molecules cm^{-3}. For minor sinks, CH_4 uptake by upland soils was derived from Fung et al. (1991) and CH_4 oxidation in the stratosphere was calculated from the archived CH_4 loss frequency described by Murray et al. (2012). The resulting atmospheric lifetime of CH_4 is about 8.9 years, consistent with the observational constraint of 9.1±0.9 years (Prather et al., 2012). We re-gridded and cropped the anthropogenic and natural CH_4 emissions in EDGAR4.2, GFED3 and Fung et al. (1991) for our nested pan-Arctic domain using the Harvard-NASA Emissions Component (HEMCO) software (Keller et al., 2014), marked as "other" in Fig. 2. Compared to CH_4 emissions from natural sources, these emissions are relatively small in 2005 (~2.1 Tg yr^{-1}).

3.3. Inversion Method

Atmospheric inversion is a procedure for using observations of atmospheric gases as constraints to estimate surface gas fluxes. The inverse problem can be characterized by solution of

$$\mathbf{y} = \mathbf{F}(\mathbf{x}) + \varepsilon \qquad (3)$$

By applying Bayesian theorem and assuming Gaussian errors, the inverse problem can be solved by minimizing the cost function, $J(\mathbf{x})$, that measures the model deviations from both prior assumptions and observations (Enting et al., 2002; Kopacz et al., 2009):

$$J(\mathbf{x}) = \left(\mathbf{F}(\mathbf{x}) - \mathbf{y}\right)^{\mathrm{T}} \mathbf{C}_{\mathrm{d}}^{-1} \left(\mathbf{F}(\mathbf{x}) - \mathbf{y}\right) + \gamma \left(\mathbf{x} - \mathbf{x}_0\right)^{\mathrm{T}} \mathbf{C}_{\mathbf{x}_0}^{-1} \left(\mathbf{x} - \mathbf{x}_0\right) \qquad (4)$$

where **y** is a vector of observations from SCIAMACHY and NOAA/ESRL, **F** is a model operator that maps emissions to observations, **x** represents CH_4 emissions to be constrained, $\mathbf{x}_0$ is the a priori estimate of **x**, $\mathbf{C}_d$ is the observational error covariance matrix that includes contributions from model error, representation error (sampling mismatch between observations and the model) and measurement error, and $\mathbf{C}_{\mathbf{x}_0}$ is the parameter error covariance matrix (containing the uncertainties of the parameters and their correlations). The regularization parameter γ controls the relative constraints applied by the observational and a priori parts of $J(\mathbf{x})$ (Kopacz et al., 2009). In the adjoint method, γ is not fixed at unity but determined by analyzing its influence on the minimum of $J(\mathbf{x})$ (Henze et al., 2007; Kopacz et al., 2009).

Minimization of $J(\mathbf{x})$ yields the following expression for the maximum a posteriori solution for the state vector $\hat{\mathbf{x}}$ and its associated error covariance $\hat{\mathbf{C}}_\mathbf{x}$ (Rodgers, 2000):

$$\hat{\mathbf{x}} = \mathbf{x}_0 + \left(\left(\nabla_\mathbf{x} \mathbf{F} \right)^T \mathbf{C}_d^{-1} \nabla_\mathbf{x} \mathbf{F} + \gamma \mathbf{C}_{\mathbf{x}_0}^{-1} \right)^{-1} \left(\nabla_\mathbf{x} \mathbf{F} \right)^T \mathbf{C}_d^{-1} \left(\mathbf{y} - \mathbf{F}\left(\mathbf{x}_0 \right) \right) \quad (5)$$

$$\hat{\mathbf{C}}_\mathbf{x}^{-1} = \left(\nabla_\mathbf{x} \mathbf{F} \right)^T \mathbf{C}_d^{-1} \nabla_\mathbf{x} \mathbf{F} + \gamma \mathbf{C}_{\mathbf{x}_0}^{-1} \quad (6)$$

where $\nabla_\mathbf{x}\mathbf{F}$ is the Jacobian matrix of the forward model. $J(\mathbf{x})$ is minimized iteratively through successive forward and backward simulations with the GEOS-Chem model and its adjoint, developed by Henze et al. (2007) and previously applied to CO, CO_2 and CH_4 source inversions (Jiang et al., 2011; Deng et al., 2014; Wecht et al., 2014). The GEOS-Chem adjoint model is a 4DVAR inverse modeling system that allows optimization of a very large number of parameters using at the same time very large sets of observational data, such as satellite data. Rather than optimizing CH_4 emissions directly, it optimizes an exponential scale factor $e_\mathbf{x}$ ($e_\mathbf{x} = \ln\left(\mathbf{x}/\mathbf{x}_0\right)$) at each grid cell to avoid negative emissions. The posterior error covariance $\hat{\mathbf{C}}_\mathbf{x}$ could be

approximated by the Davidon-Fletcher-Powell (DFP) or the Limited-memory Broyden–Fletcher–Goldfarb–Shanno (L-BFGS) optimization algorithm (Singh et al., 2011; Deng et al., 2014). But the performances of these deterministic methods are usually not promising, subjecting to the choice of initial Hessian, so-called preconditioning (Bousserez et al., 2015). In contrast, approximating $\hat{\mathbf{C}}_{\mathbf{x}}$ by stochastic methods, i.e. Monte-Carlo sampling and gradient-based randomization, could help avoid the impact of setting initial Hessian (Bousserez et al., 2015). For example, Bousserez et al. (2015) demonstrated that for high-dimensional inverse problems using a Monte Carlo stochastic approach that samples ensemble members by perturbing x_0 and y in line with $\mathbf{C}_{\mathbf{x_0}}$ and $\mathbf{C}_{\mathbf{d}}$ respectively, could guarantee a low relative error (10%) in the variance with as few as 50 members. In this study, the posterior uncertainty of nested-grid inversions was estimated using this method.

For prior emissions, their uncertainties were set as 100% in each grid box and spatial correlation was set as an e-folding function with spatial correlation lengths of 500 km at the global 4° × 5° resolution and of 300 km at the nested grid 1/2° × 2/3° resolution (Bergamaschi et al., 2009). Six global coarse-resolution inversions using different wetland emission scenarios and assimilating both surface CH_4 measurements and satellite CH_4 retrievals were performed during the period of 2005/01–2005/12. These inversions provided boundary conditions for the following nested-grid inversions. For 1/2° × 2/3° nested-grid inversions, we ran the adjoint model for 50 times over the period of 2005/07–2005/09 for each of twelve scenarios: six wetland scenarios by two data assimilation scenarios. The two data assimilation scenarios include one scenario assimilating only NOAA/ESRL measurements and another scenario assimilating both NOAA/ESRL measurements and SCIAMACHY retrievals. As described above, the 50-member ensemble run is for the calculation of posterior estimate uncertainty. The steps to construct

optimal initial conditions for global and nested inversions are described in the supplementary materials. As in Wecht et al. (2014), observations in the first week were not assimilated and each optimization was run iteratively at least 40 times until the reduction of its cost function became less than 0.5% with each successive iteration. In the GEOS-Chem adjoint model, optimization changes its course automatically if local minimum reaches.

3.4. Satellite Retrieval Bias Correction

The importance of bias correction for the assimilation of satellite retrievals has been discussed in many earlier studies (Bergamaschi et al., 2007, 2009, 2013; Fraser et al., 2013; Cressot et al., 2014; Houweling et al., 2014; Wecht et al., 2014; Alexe et al., 2015; Turner et al., 2015). Usually, these studies represented satellite retrieval bias as a regression function of one proxy parameter, i.e. latitude, air mass factor or specific humidity. Air mass factor was used as a proxy parameter by some studies due to its correlation to spectroscopic errors and residual aerosol errors (Cressot et al., 2014; Houweling et al., 2014) and specific humidity was used because water vapor is the main cause of SCIAMACHY seasonal bias that lags the variations of solar zenith angle (Houweling et al., 2014). Relative to air mass factor and humidity, latitude can represent the changes in both solar zenith angle and climate variables (Bergamaschi et al., 2007, 2009 and 2013) and thus was used by more studies. Considering that different proxies can account for different errors, the system bias of satellites may be better represented by multiple proxy parameters.

To test this hypothesis, we compared the performance of three traditional one-proxy methods (latitude φ, air mass factor A_F, specific humidity H_S) and two new two-proxy methods (latitude + humidity, air mass factor + humidity), listed in Table 1. These methods were

evaluated using two reference values: the difference between the satellite-retrieved and the GEOS-Chem modeled CH_4 column mixing ratios and the Bayesian Information Criterion (BIC) score. The BIC criterion is widely used for regression model selection and aims to award a model that fit measurements with the least model parameters. In the study, we would select the bias correction method that gives the smallest difference and the lowest BIC score. In our experiments, all bias correction functions were updated monthly. As listed in Table 1, the "latitude only" correction performs the best among the three single-proxy correction methods and is only slightly worse than the "latitude + humidity" correction method. The "air mass factor only" method does not work as well in our experiment. Turner et al. (2015) suggested that it could be attributed to a potential bias in the GEOS-Chem simulation of CH_4 in the polar stratosphere. As the "latitude + humidity" method has the smallest model-data difference and the lowest BIC score, we applied it for satellite bias correction in all global inversions.

For SCIAMACHY retrievals overpassing the pan-Arctic, because the modeled atmospheric CH_4 could be less reliable, we used another bias correction method. According to a comparison between SCIAMACHY and the high-precision Total Carbon Column Observing Network (TCCON) measurements, the system bias of SCIAMACHY retrievals could be closely correlated with specific humidity averaged over the lowest 3 km of the atmosphere (Houweling et al., 2014). And Wecht et al. (2014) has demonstrated that this humidity-proxy method shows promising performance in debiasing SCIAMACHY retrievals overpassing North America. In this study, we sought a similar linear regression relationship between SCIAMACHY bias and specific humidity. First, we detected the SCIAMACHY bias by comparing SCIAMACHY retrievals with CH_4 vertical profiles measured by the NOAA/ESRL aircraft mission over Alaska, USA, the NIES aircraft mission over Siberia, Russia and the NASA/ARCTAS aircraft mission

over Alberta, Canada. Before comparison, these CH_4 vertical profiles had been mapped to the SCIAMACHY retrieval pressure grid using Eq. (1) and (2). Fig. 3 (left) shows that the retrieved system bias (ΔXCH_4) has a negative relationship with air humidity. Because the pan-Arctic is normally dry, SCIAMACHY retrievals could be lower than atmospheric CH_4 column average mixing ratios in most of days.

After bias correction, the error variances of SCIAMACHY retrievals were estimated using the relative residual error (RRE) method described by Heald et al. (2004). Fig. S2 shows the error variances of SCIAMACHY retrievals in the global scale and Fig. 3 (right) shows the error variances in the nested grid. In both global and nested grid inversions, the total error of individual SCIAMACHY retrievals is assumed to be at least 1.5% (Bergamaschi et al., 2007; Frankenberg et al., 2011). The observational error of the NOAA/ESRL CH_4 mixing ratios is estimated as the sum of measurement error (~0.2%) and representation error. Similar to satellite retrievals, the representation error of surface measurements is defined as the standard deviation of surface CH_4 concentration differences between NOAA/ESRL measurements and GEOS-Chem.

4. Results and Discussion

4.1. Optimized Global CH_4 Emissions

As listed in Table 2, when both NOAA/ESRL measurements and SCIAMACHY retrievals were assimilated, the posterior estimates of total emissions in 2005 show good convergence at a narrow range of 496.4–511.5 Tg CH_4 yr^{-1}, albeit our six prior scenarios span in a wide range (471.5–627.8 Tg CH_4 yr^{-1}). Because the total of global emissions is constrained by the atmospheric CH_4 burden and lifetime, this convergence probably suggests that surface

376 measurements from the NOAA/ESRL network are of sufficient density and accuracy to represent
377 the global CH_4 burden if the CH_4 lifetime is correct. In contrast, the posterior CH_4 emissions
378 differ largely between different wetland emission scenarios in the TransCom3 land regions. For
379 example, in the DLEM inversion, the estimated CH_4 emissions from the Eurasian temperate
380 region are as large as 146.1 Tg CH_4 yr^{-1}. But in the CLM inversion, the total of these emissions is
381 only 84.9 Tg CH_4 yr^{-1}. Also, for CH_4 emissions from the South American tropical region, the
382 estimate is 31.4 Tg CH_4 yr^{-1} in the DLEM inversion but nearly two times larger (62.3 Tg CH_4 yr^{-1})
383 in the SDGVM inversion. There are several possible explanations for the large differences
384 between the scenarios: high-precision surface measurements could be not of sufficient density in
385 regional scales, satellite retrievals could be not of sufficient accuracy, and the GEOS-Chem
386 model and its priors could be not of high temporal and spatial resolutions to resolve satellite
387 retrievals. A detailed comparison between our estimates and previous inversion studies at the
388 global scale is presented in the supplementary materials.

389 **4.2. Optimized pan-Arctic CH_4 Emissions**

390 **4.2.1. Regional CH_4 Emissions**

391 When using both surface measurements and satellite retrievals, our estimated CH_4
392 emissions over the pan-Arctic are in the range of 11.9–28.5 Tg CH_4 yr^{-1}. The simulation is the
393 largest in the ORCHIDEE scenario and the smallest in the SDGVM scenario: 24.9±3.6 Tg CH_4
394 yr^{-1} and 16.1±4.2 Tg CH_4 yr^{-1}, respectively. Regionally, posterior CH_4 emissions from Alaska,
395 northern Canada, northern Europe and Siberia are 0.3–3.4 Tg CH_4 yr^{-1}, 1.3–7.9 Tg CH_4 yr^{-1}, 0.8–
396 8.1 Tg CH_4 yr^{-1} and 4.4–14.9 Tg CH_4 yr^{-1}, respectively. Same as the global inversions, the
397 difference of the nested-grid inversions between different scenarios is much larger than the total
398 uncertainty of priors and observations of each scenario: 16.6 Tg CH_4 yr^{-1} vs. 5.5 Tg CH_4 yr^{-1}. In

these regions, CH_4 emissions from Siberia are more uncertain (Fig. 5), a possible indication of the lack of high-quality measurements in Siberia for assimilation. Our results also indicate that the assimilation of SCIAMACHY retrievals overpassing the pan-Arctic can reduce the estimate uncertainty. For example, for the BERN scenario, the posterior uncertainty is about 18%, much smaller than the inversion that only assimilates NOAA/ESRL measurements (27%). And for the CLM scenario, the posterior uncertainty increases from 16% to 23% when only surface measurements were assimilated. Our estimates are consistent with other inverse modeling estimates. For example, Kirschke et al. (2013) reviewed a series of top-down estimation of CH_4 emissions and suggested that CH_4 emissions north of 60°N could be in the range of 12–28 Tg CH_4 yr^{-1}, very close to our estimate. This consistency could reflect the robustness of our nested-grid GEOS-Chem adjoint model and the good constraint of the NOAA/ESRL sites over the pan-Arctic on the atmospheric CH_4 field. Our estimates also imply that CH_4 emission from the pan-Arctic could constitute a large fraction of CH_4 emissions in the northern high latitudes (> 50°N). Based on the estimate (50 Tg CH_4 yr^{-1}) of Monteil et al. (2013), we calculated that 29.2-60.8% of CH_4 emissions in the northern high latitudes could be emitted from the pan-Arctic (> 60°N). For all scenarios, the inverse modeling adjusts total CH_4 emissions downward compared to prior emissions. It is possible that CH_4 emissions are overestimated by the biogeochemical models or double counted between the wetland and lake models or both. This adjustment could also be explained by the underestimate of CH_4 absorption by soils in biogeochemical models due to the missing of high-affinity methanotrophy (Oh et al., 2016).

4.2.2. CH_4 Emissions from Pan-Arctic Lakes

In contrast to CH_4 emissions from pan-Arctic wetlands, CH_4 emissions from pan-Arctic lakes at large spatial scales are still largely unknown. Consensus has not been reached yet on

how to apply the knowledge learnt from individual lakes to the pan-Arctic scale, because even lakes in a small area could have much different transport pathways (ebullition vs. diffusion), morphology (deep vs. shallow and large vs. small), eutrophication (eutrophic vs. oligotrophic) and carbon source (thermokarst vs. non-thermokarst and yedoma vs. non-yedoma). Because wetlands and lakes, both inundation landscapes, are usually neighbored, it is difficult to use inverse modeling at coarse spatial scales to detect strong CH_4 emissions that are emitted solely by lakes. To test whether high-resolution inversions can better represent CH_4 emissions from lakes, we conducted a comparison test ("DLEM only") over the East Siberia Coastal Lowlands (Fig. 1) using the DLEM model and excluding CH_4 emissions from lakes. We chose the East Siberia Lowlands to test our hypothesis as lakes there occupy 56% of the water-inundated landscapes, i.e. lakes, wetlands and rivers (Lehner and Döll, 2004) and a large fraction of lakes in the region are high-flux yedoma lakes (Walter et al., 2006). We chose the DLEM model considering that the simulated wetland CH_4 emissions in this model are weak for the East Siberia Lowlands. This design is also aimed to alleviate the impact of one major shortcoming: because there are not sufficient high-quality observations, we optimized CH_4 emission in each grid cell separately for wetlands and lakes and in this manner a fraction of lake emissions could be attributed incorrectly to wetlands or vice versa. The inversion of the "DLEM only" scenario is shown in Fig. S5. In comparison to Fig. 4c, CH_4 emissions from the East Siberia Coastal Lowlands are low in Fig. S5. A further comparison of model-satellite agreement between the DLEM scenario and this no-lake scenario reveals that the agreement improves when lake emissions are considered (see Fig. 6; $p = 0.0032838$ at the two-sample t-test). It implies that CH_4 emissions from regional lakes could be significant. As illustrated above, however, the spatial neighborhood of wetlands and lakes makes it difficult to conduct similar experiments in other

areas. Thus we are cautious to claim that CH_4 emissions from lakes are ubiquitously strong across the pan-Arctic. Rather, since we used six wetland models that can simulate very different wetland emission distributions at spatial and temporal scales, our estimates of 2.4–14.2 Tg CH_4 yr^{-1} for lake emissions could be more useful in explaining the range of this source. The lower bound of our estimate is much smaller than the estimate of 7.1–17.3 Tg CH_4 yr^{-1} by Bastviken et al. (2011) in the use of extensive site-level observations. In contrast, the upper bound of our estimate is within the range. Given the wide span of this estimate, it is difficult to say whether CH_4 emissions from pan-Arctic lakes can be significant across the region.

4.2.3. CH_4 Emissions from Pan-Arctic Wetlands

Arctic tundra is regarded as an important source of CH_4 in the northern high latitudes. By using process-based models and atmospheric CH_4 observations, McGuire et al. (2012) estimated that Arctic tundra was a source of 25 Tg CH_4 yr^{-1} to the atmosphere during 1990–2006. By using the TM5-4DVAR inverse model and assimilating SCIAMACHY and NOAA/ESRL observations, Alexe et al. (2015) estimated that CH_4 emissions from Arctic wetlands were 18.2 Tg CH_4 yr^{-1} for 2010–2011. A similar estimate of 16±5 Tg CH_4 yr^{-1} was also made by Bruhwiler et al. (2014) using the CarbonTracker-CH_4 assimilation system. Our estimate of 5.5–14.2 Tg CH_4 yr^{-1} overlaps with the estimate of Bruhwiler et al. (2014) but is much lower than the estimates of Alexe et al. (2015) and McGuire et al. (2012). However, McGuire et al. (2012) did not use complex inverse models and Alexe et al. (2015) used the coarse-resolution TM5-4DVAR inverse model. As our global inversions (Table 2) are consistent with the estimate of Alexe et al. (2015), this difference is likely introduced by the use of the nested-grid inverse model. In other words, the nested-grid inverse model reveals some information that could be missed in global coarse-resolution inversions. For Siberian wetlands, they could emit much more CH_4 (1.6–7.6 Tg yr^{-1})

than any other areas. But the uncertainty of this source is also the largest. Using the atmospheric CH_4 observation data at several sites near to Siberian wetlands, Berchet et al. (2015) estimated that CH_4 emissions from Siberian wetlands were in the range of 1–13 Tg CH_4 yr^{-1}, wider than our estimated range. In addition, our estimate is also much smaller than the estimate of 21.63 ± 5.25 Tg CH_4 yr^{-1} by Kim et al. (2012) for annual mean CH_4 emissions from Siberian wetlands during 2005–2010. According to our inversions, CH_4 emissions from wetlands in Alaska, northern Canada, northern Europe are 0–1.2 Tg CH_4 yr^{-1}, 0.4–4.8 Tg CH_4 yr^{-1} and 0.7–3.6 Tg CH_4 yr^{-1}, respectively. For Alaskan wetlands, the total of posterior CH_4 emissions is much lower than the inferred value of 4.1 Tg CH_4 yr^{-1} for the Alaskan Yukon River basin during 1986–2005 using the modeling of process-based CH_4 biogeochemistry and large-scale hydrology (Lu and Zhuang, 2012) and also much lower than the inferred value of 3 Tg CH_4 yr^{-1} for the whole Alaska (Zhuang et al., 2007). Our estimate of wetland emissions from northern Europe compasses a European-scale estimate of 3.6 Tg CH_4 yr^{-1} by Saarnio et al. (2009), agreeing with the investigation that wetlands in Europe are predominantly located north of 60°N.

4.2.4. Evaluation of Pan-Arctic CH_4 Inversions

As shown in Fig. 7, in most of scenarios, the nested grid inversions perform much better than both the forward simulations and the global inversions at NOAA/ESRL pan-Arctic flask sites (Fig. 1). For example, for the ORCHIDEE scenario, the nested grid inversion reduces the model bias by 44 ppb relative to the forward run and by 20 ppb relative to the global inversion, respectively. Also, for the SDGVM scenario, it reduces the model bias by 22 ppb relative to the forward run and by 13 ppb relative to the global inversion, respectively. But for aircraft CH_4 measurements, it is more complex. The nested grid inversions can reduce the model bias in some scenarios greatly, i.e. the CLM4Me scenario and the SDGVM scenario. But in many cases, they

do not perform visibly better than the forward runs and the global inversions. One possible reason is that the aircraft CH_4 RMS has already been low and thus the remaining errors, including the representation error of model diurnal variability, cannot be resolved by our current inversion system. For example, CH_4 emissions from Alaska can be well constrained by three NOAA/ESRL surface sites in Alaska (BRW, CBA and SHM) and the CH_4 mixing ratios at the aircraft PFA site are representative of the interior of Alaska as pointed out in Sweeney et al. (2015). It is also possible that the increase of grid cells in the nested grid inversions introduced more transport and computation errors.

4.3. Further Discussion

Both the global and nested-grid inversions indicate that the inverse modeling is more sensitive to different wetland models than prior emission error and data error. Thus, to gain better understandings of the global and pan-Arctic CH_4 cycles, it is important to develop more realistic biogeochemical models. Especially, from the perspective of inverse modeling, focus should be on improving the spatial and temporal representation of the models rather than emission magnitude.

For the high-resolution inverse modeling, transport and computation errors of the nested-grid CTMs need to be reduced for better performance. These CTMs can also benefit the efforts to assimilate aircraft CH_4 measurements. For the purpose of satellite data bias correction, more coordination between satellite missions and aircraft missions is demanded. The treatment of the SCIAMACHY bias could be an important uncertainty source for our estimates, as suggested by Houweling et al. (2014). Future top-down studies could benefit from a more reasonable bias correction method, even for low bias satellite products, e.g. GOSAT (Alexe et al., 2015).

The attribution of CH_4 fluxes to spatially overlapped sources, e.g. wetlands and lakes, could be problematic for even high-resolution inversions. Carbon isotope measurements ($\delta^{13}CH_4$) are widely used to separate biogenic and geologic CH_4 sources (Langenfelds et al., 2002) but are not useful for two biogenic sources with similar carbon isotope ratios (Walter et al., 2008; Fisher et al., 2011). In our study, lake and wetland emissions were simulated separately by different models. This raised the possibility of double counting emissions of the two sources. A possible solution is to simulate them together in one earth system model and use a consistent method to identify wetland and lake pixels.

Our nested grid adjoint model currently does not cover the regions near the North Pole. While it could be rare in the summer time, if air mass transports across the Arctic Ocean, it may not be represented in the model. In the following studies, we will adapt the advection algorithm for the polar region from the global adjoint model to the nested-grid model and validate the adaptation. These refinements shall reduce the uncertainty of our estimates. It is also valuable to discuss the integration of other natural CH_4 sources found in the pan-Arctic, such as CH_4 emission from subsea permafrost of East Siberian shelf (Berchet et al., 2016; Thornton et al., 2016). As shown in Fig. 1, our inverse modeling assimilated few high-precision surface CH_4 measurements in Siberia and northern Canada. Since some efforts have already been made by different teams to measure atmospheric CH_4 routinely in Siberia (e.g., the JR-STATION network by NIES, the Zotino Tall Tower Observatory by MPI-BGC and the Tiksi site by the Finnish Meteorological Institute) and in North American Arctic (e.g., the Behchoko site by Environment Canada), we would like to take advantage of these measurements to further improve our inversion results and re-evaluate the gains of using satellite data in our future studies.

5. Conclusion

In this study, we used a high-resolution nested-grid adjoint model in the pan-Arctic domain to constrain CH_4 emissions from pan-Arctic wetlands, lakes and anthropogenic sources. The sensitivity of the method to different prior wetland CH_4 fluxes was tested. When assimilating both NOAA/ESRL measurements and SCIAMACHY retrievals, we estimated that in 2005, the total of global CH_4 emissions was in the range of 496.4–511.5 Tg CH_4 yr^{-1}, with wetlands contributing 130.0–203.3 Tg CH_4 yr^{-1}. Both of these estimates are consistent with some widely accepted expert assessments. The estimated CH_4 emissions in the pan-Arctic were in the range of 11.9–28.5 Tg yr^{-1}, with wetland and lake emissions ranging from 5.5 to 14.2 Tg yr^{-1} and from 2.4 to 14.2 Tg yr^{-1}, respectively. The largest CH_4 emissions in the pan-Arctic are from Siberian wetlands and lakes. The study demonstrates that the assimilation of satellite retrievals can reduce the uncertainty of the nested grid inversions. Evaluation with independent datasets shows that the nested inversions can better improve the representation of CH_4 mixing ratios in lower boundary layer rather than top boundary layer and free troposphere.

Acknowledgements: We would like to thank the two anonymous reviewers for their thorough and constructive reviews. Many thanks are given to the WETCHIMP investigators for making their simulations of wetland methane emissions available. We appreciate the help from Guang-Dih Lei and Bhagirath M. Trivedi at NASA and Robert Yantosca at Harvard for processing nested grid GOES-5 met data and the help from Christoph A. Keller at Harvard for processing nested grid emission data by HEMCO. This study is supported through projects funded to Q. Z. by the NASA Land Use and Land Cover Change program (NASA-NNX09AI26G), Department of Energy (DE-FG02-08ER64599), the NSF Division of Information and Intelligent Systems (NSF-1028291), and the NSF Carbon and Water in the Earth Program (NSF-0630319). This

research is also in part supported by the Director, Office of Science, Office of Biological and Environmental Research of the US Department of Energy under Contract No. DE-AC02-05CH11231 as part of their Earth System Modeling Program. D. K. H. acknowledges NOAA grant no. NA14OAR4310136. A. J. T. was supported by a Department of Energy (DOE) Computational Science Graduate Fellowship (CSGF). The supercomputing resource is provided by Rosen Center for Advanced Computing at Purdue University.

References

Alexe, M., Bergamaschi, P., Segers, A., Detmers, R., Butz, A., Hasekamp, O., Guerlet, S., Parker, R., Boesch, H., Frankenberg, C., Scheepmaker, R. A., Dlugokencky, E., Sweeney, C., Wofsy, S. C. and Kort, E. A.: Inverse modeling of CH_4 emissions for 2010–2011 using different satellite retrieval products from GOSAT and SCIAMACHY, Atmos. Chem. Phys., 15, 113–133, doi:10.5194/acp-15-113-2015, 2015.

Aydin, M., Verhulst, K. R., Saltzman, E. S., Battle, M. O., Montzka, S. A, Blake, D. R., Tang, Q. and Prather, M. J.: Recent decreases in fossil-fuel emissions of ethane and methane derived from firn air, Nature, 476(7359), 198–201, 2011.

Bastviken, D., Tranvik, L., Downing, J., Crill, P. M. and Enrich-Prast, A.: Freshwater methane emissions offset the continental carbon sink, Science, 331, 50–50, 2011.

Berchet, A., Pison, I., Chevallier, F., Paris, J.-D., Bousquet, P., Bonne, J.-L., Arshinov, M. Y., Belan, B. D., Cressot, C., Davydov, D. K., Dlugokencky, E. J., Fofonov, A. V., Galanin, A., Lavrič, J., Machida, T., Parker, R., Sasakawa, M., Spahni, R., Stocker, B. D. and Winderlich, J.:

580 Natural and anthropogenic methane fluxes in Eurasia: a meso-scale quantification by generalized
581 atmospheric inversion, Biogeosciences, 12, 5393–5414, doi:10.5194/bg-12-5393-2015, 2015.

582 Berchet, A., Bousquet, P., Pison, I., Locatelli, R., Chevallier, F., Paris, J.-D., Dlugokencky, E. J.,
583 Laurila, T., Hatakka, J., Viisanen, Y., Worthy, D. E. J., Nisbet, E. G., Fisher, R. E., France, J. L.,
584 Lowry, D. and Ivakhov, V.: Atmospheric constraints on the methane emissions from the East
585 Siberian Shelf, Atmos. Chem. Phys., 16, 4147–4157, doi:10.5194/acp-16-4147-2016, 2016.

586 Bergamaschi, P., Krol, M., Dentener, F., Vermeulen, A., Meinhardt, F., Graul, R., Ramonet, M. ,
587 Peters, W. and Dlugokencky, E. J.: Inverse modelling of national and European CH_4 emissions
588 using the atmospheric zoom model TM5, Atmos. Chem. Phys., 5, 2431–2460, 2005.

589 Bergamaschi, P., Frankenberg, C., Meirink, J. F., Krol, M., Dentener, F., Wagner, T., Platt, U.,
590 Kaplan, J. O., Körner, S., Heimann, M., Dlugokencky, E. J. and Goede, A.: Satellite
591 chartography of atmospheric methane from SCIAMACHY on board ENVISAT: 2. Evaluation
592 based on inverse model simulations, J. Geophys. Res., 112, D02304, doi:10.1029/2006JD007268,
593 2007.

594 Bergamaschi, P., Frankenberg, C., Meirink, J. F., Krol, M., Villani, M. G., Houweling, S.,
595 Dentener, F., Dlugokencky, E. J., Miller, J. B., Gatti, L. V., Engel, A. and Levin, I.: Inverse
596 modeling of global and regional CH4 emissions using SCIAMACHY satellite retrievals, J.
597 Geophys. Res., 114, D22301, doi:10.1029/2009JD012287, 2009.

598 Bergamaschi, P., Houweling, S., Segers, A., Krol, M., Frankenberg, C., Scheepmaker, R. A.,
599 Dlugokencky, E., Wofsy, S. C., Kort, E. a., Sweeney, C., Schuck, T., Brenninkmeijer, C., Chen,
600 H., Beck, V. and Gerbig, C.: Atmospheric CH4 in the first decade of the 21st century: Inverse

modeling analysis using SCIAMACHY satellite retrievals and NOAA surface measurements, J. Geophys. Res. Atmos., 118, 1-20, doi:10.1002/jgrd.50480, 2013.

Bey, I., Jacob, D. J., Yantosca, R. M., Logan, J. A., Field, B. D., Fiore, A. M., Li, Q., Liu, H. Y., Mickley, L. J., and Schultz, M. G.: Global modeling of tropospheric chemistry with assimilated meteorology: model description and evaluation, J. Geophys. Res., 106, 23073-23095, 2001.

Bloom, A. A., Palmer, P. I., Fraser, A., Reay, D. S. and Frankenberg, C.: Large-Scale Controls of Methanogenesis Inferred from Methane and Gravity Spaceborne Data, Science, 327, 322–325, doi:10.1038/nchem.467, 2010.

Bousquet, P., Ciais, P., Miller, J. B., Dlugokencky, E. J., Hauglustaine, D. A, Prigent, C., Van der Werf, G. R., Peylin, P., Brunke, E.-G., Carouge, C., Langenfelds, R. L., Lathière, J., Papa, F., Ramonet, M., Schmidt, M., Steele, L. P., Tyler, S. C. and White, J.: Contribution of anthropogenic and natural sources to atmospheric methane variability, Nature, 443(7110), 439–443, doi:10.1038/nature05132, 2006.

Bousserez, N., Henze, D. K., Perkins, A., Bowman, K. W., Lee, M., Liu, J., Deng, F. and Jones, D. B. A.: Improved analysis-error covariance matrix for high-dimensional variational inversions: application to source estimation using a 3D atmospheric transport model, Q. J. R. Meteorol. Soc., doi:10.1002/qj.2495, 2015.

Bruhwiler, L. M., Dlugokencky, E., Masarie, K., Ishizawa, M., Andrews, A., Miller, J., Sweeney, C., Tans, P. and Worthy, D.: CarbonTracker-CH_4: an assimilation system for estimating emissions of atmospheric methane, Atmos. Chem. Phys., 14, 8269–8293, doi:10.5194/acp-14-8269-2014, 2014.

622 Butz, A., Hasekamp, O. P., Frankenberg, C., Vidot, J., and Aben, I.: CH_4 retrievals from space-
623 based solar backscatter measurements: Performance evaluation against simulated aerosol and
624 cirrus loaded scenes, J. Geophys. Res. Atmos., 115, D24302, doi:10.1029/2010JD014514, 2010.

625 Cressot, C., Chevallier, F., Bousquet, P., Crevoisier, C., Dlugokencky, E. J., Fortems-Cheiney,
626 A., Frankenberg, C., Parker, R., Pison, I., Scheepmaker, R. A., Montzka, S. A., Krummel, P. B.,
627 Steele, L. P. and Langenfelds, R. L.: On the consistency between global and regional methane
628 emissions inferred from SCIAMACHY, TANSO-FTS, IASI and surface measurements, Atmos.
629 Chem. Phys., 14, 577–592, doi:10.5194/acp-14-577-2014, 2014.

630 Deng, F., Jones, D. B. A., Henze, D. K., Bousserez, N., Bowman, K. W., Fisher, J. B., Nassar, R.,
631 O'Dell, C., Wunch, D., Wennberg, P. O., Kort, E. A., Wofsy, S. C., Blumenstock, T., Deutscher,
632 N. M., Griffith, D. W. T., Hase, F., Heikkinen, P., Sherlock, V., Strong, K., Sussmann, R. and
633 Warneke, T.: Inferring regional sources and sinks of atmospheric CO_2 from GOSAT XCO_2 data,
634 Atmos. Chem. Phys., 14, 3703–3727, doi:10.5194/acp-14-3703-2014, 2014.

635 Denman, K. L., Brasseur, G., Chidthaisong, A., Ciais, P., Cox, P. M., Dickinson, R. E.,
636 Hauglustaine, D., Heinze, C., Holland, E., Jacob, D., Lohmann, U., Ramachandran, S., da Silva
637 Dias, P. L., Wofsy, S. C., and Zhang, X.: Couplings Between Changes in the Climate System and
638 Biogeochemistry. In: Climate Change 2007: The Physical Science Basis. Contribution of
639 Working Group I to the Fourth Assessment Report of the Intergovernmental Panel on Climate
640 Change, edited by Solomon, S., Qin, D., Manning, M., Chen, Z., Marquis, M., Averyt, K. B.,
641 Tignor, M., and Miller, H. L., Cambridge University Press, Cambridge, United Kingdom and
642 New York, N. Y., USA, 2007.

643 Dlugokencky, E., Masarie, K. and Lang, P.: Continuing decline in the growth rate of atmospheric
644 methane burden, Nature, 393, 447–450, 1998.

645 Dlugokencky, E. J., Houweling, S., Bruhwiler, L., Masarie, K. A., Lang, P. M., Miller, J. B, and
646 Tans, P. P.: Atmospheric methane levels off: Temporary pause or a new steady-state?, Geophys.
647 Res. Lett., 30, No. 19, doi: 10.1029/2003GL018126, 2003.

648 Dlugokencky, E. J., Myers, R. C., Lang, P. M., Masarie, K. A., Crotwell, A. M., Thoning, K. W.,
649 Hall, B. D., Elkins, J. W., and Steele, L. P.: Conversion of NOAA atmospheric dry-air CH_4 mole
650 fractions to a gravimetrically prepared standard scale, J. Geophys. Res. Atmos., 110, D18306,
651 doi:10.1029/2005JD006035, 2005.

652 Dlugokencky, E. J., Bruhwiler, L., White, J. W. C., Emmons, L. K., Novelli, P. C., Montzka, S.
653 A., Masarie, K. A., Lang, P. M., Crotwell, A. M., Miller, J. B. and Gatti, L. V.: Observational
654 constraints on recent increases in the atmospheric CH_4 burden, Geophys. Res. Lett., 36, L18803,
655 doi:10.1029/2009GL039780, 2009.Dlugokencky, E. J., Lang, P. M., Crotwell, A.M., Masarie,
656 K.A. and Crotwell M.J.: Atmospheric Methane Dry Air Mole Fractions from the NOAA ESRL
657 Carbon Cycle Cooperative Global Air Sampling Network, 1983-2013, Version: 2014-06-24,
658 ftp://aftp.cmdl.noaa.gov/data/trace_gases/ch4/flask/surface/ (last access: 9 June 2015), 2014.

659 Enting, I. G.: Inverse problems in atmospheric constituent transport, Cambridge University Press,
660 2002.

661 Etheridge, D. M., Steele, L. P., Francey, R. J., and Langenfelds, R. L.: Atmospheric methane
662 between 1000 A.D. and present: Evidence of anthropogenic emissions and climatic variability, J.
663 Geophys. Res., 103(D13), 15,979-15,993, 1998.

European Commission, Joint Research Centre/Netherlands Environmental Assessment Agency: Emission Database for Global Atmospheric Research (EDGAR), release version 4.0., http://edgar.jrc.ec.europa.eu (last access: 11 June 2015), 2009.

Fiore, A. M., Horowitz, L. W., Dlugokencky, E. J. and West, J. J.: Impact of meteorology and emissions on methane trends, 1990–2004, Geophys. Res. Lett., 33, L12809, doi:10.1029/2006GL026199, 2006.

Fisher, R. E., Sriskantharajah, S., Lowry, D., Lanoisellé, M., Fowler, C. M. R., James, R. H., Hermansen, O., Lund Myhre, C., Stohl, A., Greinert, J., Nisbet-Jones, P. B. R., Mienert, J. and Nisbet, E. G.: Arctic methane sources: Isotopic evidence for atmospheric inputs, Geophys. Res. Lett., 38, L21803, doi:10.1029/2011GL049319, 2011.

Frankenberg, C., Meirink, J. F., Bergamaschi, P., Goede, A. P. H., Heimann, M., Kröner, S., Platt, U., van Weele, M., and Wagner, T.: Satellite chartography of atmospheric methane from SCIAMACHY on board ENVISAT: Analysis of the years 2003 and 2004, J. Geophys. Res., 111, D07303, doi:10.1029/2005JD006235, 2006.

Frankenberg, C., Bergamaschi, P., Butz, A., Houweling, S., Meirink, J. F., Notholt, J., Petersen, A. K., Schrijver, H., Warneke, T., and I. Aben: Tropical methane emissions: A revised view from SCIAMACHY onboard ENVISAT, Geophys. Res. Lett., 35, L15811, doi:10.1029/2008GL034300, 2008.

Frankenberg, C., Aben, I., Bergamaschi, P., Dlugokencky, E. J., van Hees, R., Houweling, S., van der Meer, P., Snel, R., and Tol, P.: Global column-averaged methane mixing ratios from 2003 to 2009 as derived from SCIAMACHY: Trends and variability, J. Geophys. Res., 116, D02304, doi:10.1029/2010JD014849, 2011.

686 Fraser, A., Palmer, P. I., Feng, L., Boesch, H., Cogan, A., Parker, R., Dlugokencky, E. J., Fraser,
687 P. J., Krummel, P. B., Langenfelds, R. L., O'Doherty, S., Prinn, R. G., Steele, L. P., van der
688 Schoot, M. and Weiss, R. F.: Estimating regional methane surface fluxes: the relative importance
689 of surface and GOSAT mole fraction measurements, Atmos. Chem. Phys., 13, 5697–5713,
690 doi:10.5194/acp-13-5697-2013, 2013.

691 Fung, I., John, J., Lerner, J., Matthews, E., Prather, M., Steele, L. P., and Fraser, P. J.: Three-
692 dimensional model synthesis of the global methane cycle, J. Geophys. Res., 96, 13,033–13,065,
693 doi:10.1029/91JD01247, 1991.

694 GLOBALVIEW-CH4: Cooperative Atmospheric Data Integration Project - Methane. CD-ROM,
695 NOAA ESRL, Boulder, Colorado, available at: ftp://ftp.cmdl.noaa.gov (last access: 19 August
696 2015), Path: products/globalview/ch4, 2009.

697 Gurney, K. R., Law, R. M., Denning, A. S., Rayner, P. J., Baker, D., Bousquet, P., Bruhwiler, L.,
698 Chen, Y.-H., Ciais, P., Fan, S., Fung, I. Y., Gloor, M., Heimann, M., Higuchi, K., John, J., Maki,
699 T., Maksyutov, S., Masarie, K., Peylin, P., Prather, M., Pak, B. C., Randerson, J., Sarmiento, J.,
700 Taguchi, S., Takahashi, T., and Yuen, C.-W.: Towards robust regional estimates of CO_2 sources
701 and sinks using atmospheric transport models, Nature, 415, 626–630, doi:10.1038/415626a, 2002.

702 Heald, C. L., Jacob, D. J., Jones, D. B. A., Palmer, P. I., Logan, J. A., Streets, D. G., Sachse, G.
703 W., Gille, J. C., Hoffman, R. N. and Nehrkorn, T.: Comparative inverse analysis of satellite
704 (MOPITT) and aircraft (TRACE-P) observations to estimate Asian sources of carbon monoxide,
705 J. Geophys. Res., 109, D23306, doi:10.1029/2004JD005185, 2004.

706 Henze, D. K., Hakami, A., and Seinfeld, J. H.: Development of the adjoint of GEOS-Chem,
707 Atmos. Chem. Phys., 7, 2413–2433, 2007.

Houweling, S., Krol, M., Bergamaschi, P., Frankenberg, C., Dlugokencky, E. J., Morino, I., Notholt, J., Sherlock, V., Wunch, D., Beck, V., Gerbig, C., Chen, H., Kort, E. a., Röckmann, T. and Aben, I.: A multi-year methane inversion using SCIAMACHY, accounting for systematic errors using TCCON measurements, Atmos. Chem. Phys., 14, 3991–4012, doi:10.5194/acp-14-3991-2014, 2014.

Jiang, Z., Jones, D. B. A., Kopacz, M., Liu, J., Henze, D. K., and Heald, C.: Quantifying the impact of model errors on top-down estimates of carbon monoxide emissions using satellite observations, J. Geophys. Res., 116, D15306, doi:10.1029/2010JD015282, 2011.

Kai, F. M., Tyler, S. C., Randerson, J. T. and Blake, D. R.: Reduced methane growth rate explained by decreased Northern Hemisphere microbial sources, Nature, 476(7359), 194–197, doi:10.1038/nature10259, 2011.

Kaminski, T. and Heimann, M.: Inverse modeling of atmospheric carbon dioxide fluxes, Science, 294, 259–259, 2001.

Keller, C. A., Long, M. S., Yantosca, R. M., Da Silva, A. M., Pawson, S., and Jacob, D. J.: HEMCO v1.0: a versatile, ESMF-compliant component for calculating emissions in atmospheric models, Geosci. Model Dev., 7, 1409-1417, doi:10.5194/gmd-7-1409-2014, 2014.

Khalil, M. A. K., Butenhoff, C. L. and Rasmussen, R. A.: Atmospheric methane: trends and cycles of sources and sinks, Environ. Sci. Technol., 41, 2131–2137, 2007.

Kim, H., Machida, T., Sasakawa, M., Belikov, D., Saeki, T., Ito, A. and Maksyutov, S.: Recent variation of Siberian CH_4 fluxes estimated from atmospheric observations of CH_4, AGU Fall Meeting Abstracts, 1, GC24A-08, 2012.

729 Kirschke, S., Bousquet, P., Ciais, P., Saunois, M., Canadell, J. G., Dlugokencky, E. J.,
730 Bergamaschi, P., Bergmann, D., Blake, D. R., Bruhwiler, L., Cameron-Smith, P., Castaldi, S.,
731 Chevallier, F., Feng, L., Fraser, A., Heimann, M., Hodson, E. L., Houweling, S., Josse, B., Fraser,
732 P. J., Krummel, P. B., Lamarque, J.-F., Langenfelds, R. L., Le Quéré, C., Naik, V., O'Doherty,
733 S., Palmer, P. I., Pison, I., Plummer, D., Poulter, B., Prinn, R. G., Rigby, M., Ringeval, B.,
734 Santini, M., Schmidt, M., Shindell, D. T., Simpson, I. J., Spahni, R., Steele, L. P., Strode, S. A.,
735 Sudo, K., Szopa, S., van der Werf, G. R., Voulgarakis, A., van Weele, M., Weiss, R. F.,
736 Williams, J. E., and Zeng, G.: Three decades of global methane sources and sinks, Nat. Geosci.,
737 6, 813–823, doi:10.1038/ngeo1955, 2013.

738 Kopacz, M., Jacob, D. J., Henze, D. K., Heald, C. L., Streets, D. G. and Zhang, Q.: Comparison
739 of adjoint and analytical Bayesian inversion methods for constraining Asian sources of carbon
740 monoxide using satellite (MOPITT) measurements of CO columns, J. Geophys. Res., 114,
741 D04305, doi:10.1029/2007JD009264, 2009.

742 Kort, E. A., Wofsy, S. C., Daube, B. C., Diao, M., Elkins, J. W., Gao, R. S., Hintsa, E. J., Hurst,
743 D. F., Jimenez, R., Moore, F. L., Spackman, J. R. and Zondlo, M. A.: Atmospheric observations
744 of Arctic Ocean methane emissions up to 82° north, Nat. Geosci., 5, 1–4, doi:10.1038/ngeo1452,
745 2012.

746 Koven, C. D., Ringeval, B., Friedlingstein, P., Ciais, P., Cadule, P., Khvorostyanov, D., Krinner,
747 G. and Tarnocai, C.: Permafrost carbon-climate feedbacks accelerate global warming, Proc. Natl.
748 Acad. Sci., 108, 14769–14774, doi:10.1073/pnas.1103910108, 2011.

749 Langenfelds, R. L., Francey, R. J., Pak, B. C., Steele, L. P., Lloyd, J., Trudinger, C. M. and
750 Allison, C. E.: Interannual growth rate variations of atmospheric CO_2 and its $\delta^{13}C$, H_2, CH_4, and

751 CO between 1992 and 1999 linked to biomass burning, Global Biogeochem. Cycles, 16(3), 1048,
752 doi:10.1029/2001GB001466, 2002.

753 Lehner, B. and Döll, P.: Development and validation of a global database of lakes, reservoirs and
754 wetlands, J. Hydrol., 296, 1–22, 2004.

755 Levin, I., Veidt, C., Vaughn, B. H., Brailsford, G., Bromley, T., Heinz, R., Lowe, D., Miller, J.
756 B., Poβ, C. and White, J. W. C.: No inter-hemispheric $\delta^{13}CH_4$ trend observed, Nature, 486, E3–
757 E4, doi:10.1038/nature11175, 2012.

758 Lin, S.-J. and Rood, R. B.: Multidimensional Flux-Form Semi-Lagrangian Transport Schemes,
759 Mon. Weather Rev., 124, 2046–2070, 1996.

760 Lu, X. and Zhuang, Q.: Modeling methane emissions from the Alaskan Yukon River basin,
761 1986–2005, by coupling a large-scale hydrological model and a process-based methane model, J.
762 Geophys. Res., 117, G02010, doi:10.1029/2011JG001843, 2012.

763 Machida, T., Nakazawa, T., Muksyutov, S., Tohjima, Y., Takahashi, Y.,Watai, T., Vinnichenko,
764 N., Panchenko, M., Arshinov, M., Fedoseev, N., and Inoue, G.: Temporal and spatial variations
765 of atmospheric CO_2 mixing ratio over Siberia, paper presented at the Sixth International CO_2
766 Conference, Sendai, Japan, 1–5, 2001.

767 McGuire, A. D., Christensen, T. R., Hayes, D., Heroult, A., Euskirchen, E., Kimball, J. S.,
768 Koven, C., Lafleur, P., Miller, P. A., Oechel, W., Peylin, P., Williams, M., and Yi, Y.: An
769 assessment of the carbon balance of Arctic tundra: comparisons among observations, process
770 models, and atmospheric inversions, Biogeosciences, 9, 3185-3204, doi:10.5194/bg-9-3185-2012,
771 2012.

772 Meirink, J. F., Bergamaschi, P. and Krol, M. C.: Four-dimensional variational data assimilation
773 for inverse modelling of atmospheric methane emissions: method and comparison with synthesis
774 inversion, Atmos. Chem. Phys., 8, 6341–6353, doi:10.5194/acp-8-6341-2008, 2008.

775 Melton, J. R., et al.: Present state of global wetland extent and wetland methane modelling:
776 conclusions from a model inter-comparison project (WETCHIMP), Biogeosciences, 10, 753-788,
777 2013.

778 Meng, L., Paudel, R., Hess, P. G. M. and Mahowald, N. M.: Seasonal and interannual variability
779 in wetland methane emissions simulated by CLM4Me' and CAM-chem and comparisons to
780 observations of concentrations, Biogeosciences, 12, 4029–4049, doi:10.5194/bg-12-4029-2015,
781 2015.

782 Miller, S. M., Wofsy, S. C., Michalak, A. M., Kort, E. A., Andrews, A. E., Biraud, S. C.,
783 Dlugokencky, E. J., Eluszkiewicz, J., Fischer, M. L., Janssens-Maenhout, G., Miller, B. R.,
784 Miller, J. B., Montzka, S. A., Nehrkorn, T. and Sweeney, C.: Anthropogenic emissions of
785 methane in the United States, Proc. Natl. Acad. Sci., 110(50), 20018–20022,
786 doi:10.1073/pnas.1314392110, 2013.

787 Miller, S. M., Worthy, D. E. J., Michalak, A. M., Wofsy, S. C., Kort, E. A., Havice, T. C.,
788 Andrews, A. E., Dlugokencky, E. J., Kaplan, J. O., Levi, P. J., Tian, H. and Zhang, B.:
789 Observational constraints on the distribution, seasonality, and environmental predictors of North
790 American boreal methane emissions, Global Biogeochem. Cycles, 28, 146–160,
791 doi:10.1002/2013GB004580, 2014.

792 Miyazaki, K., Patra, P. K., Takigawa, M., Iwasaki, T. and Nakazawa, T.: Global-scale transport
793 of carbon dioxide in the troposphere, J. Geophys. Res., 113, D15301,
794 doi:10.1029/2007JD009557, 2008.

795 Monteil, G., Houweling, S., Butz, A., Guerlet, S., Schepers, D., Hasekamp, O., Frankenberg, C.,
796 Scheepmaker, R., Aben, I. and Röckmann, T.: Comparison of CH_4 inversions based on 15
797 months of GOSAT and SCIAMACHY observations, J. Geophys. Res. Atmos., 118, 1–17,
798 doi:10.1002/2013JD019760, 2013.

799 Murray, L. T., Jacob, D. J., Logan, J. A., Hudman, R. C., and Koshak, W. J.: Optimized regional
800 and interannual variability of lightning in a global chemical transport model constrained by
801 LIS/OTD satellite data, J. Geophys. Res., 117, D20307, doi:10.1029/2012JD017934, 2012.

802 Myhre, G., Shindell, D., Bréon, F.-M., Collins, W., Fuglestvedt, J., Huang, J., Koch, D.,
803 Lamarque, J.-F., Lee, D., Mendoza, B., Nakajima, T., Robock, A., Stephens, G., Takemura, T.,
804 and Zhang, H.: Anthropogenic and natural radiative forcing, in: Climate Change 2013: the
805 Physical Science Basis, contribution of Working Group I to the Fifth Assessment Report of the
806 Intergovernmental Panel on Climate Change, edited by: Stocker, T. F., Qin, D., Plattner, G.-K.,
807 Tignor, M., Allen, S. K., Boschung, J., Nauels, A., Xia, Y., Bex, V., and Midgley, P. M.,
808 Cambridge University Press, Cambridge, UK and New York, NY, USA, 2013.

809 Myhre, C. L., Ferré, B., Platt, S. M., Silyakova, A., Hermansen, O., Allen, G., Pisso, I.,
810 Schmidbauer, N., Stohl, A., Pitt, J., Jansson, P., Greinert, J., Percival, C., Fjaeraa, A. M., O'Shea,
811 S., Gallagher, M., Le Breton, M., Bower, K., Bauguitte, S., Dalsøren, S., Vadakkepuliyambatta,
812 S., Fisher, R. E., Nisbet, E. G., Lowry, D., Myhre, G., Pyle, J., Cain, M. and Mienert, J.:
813 Extensive release of methane from Arctic seabed west of Svalbard during summer 2014 does not

influence the atmosphere, Geophys. Res. Lett., 43, 4624–4631, doi:10.1002/2016GL068999, 2016.

Nisbet, E. G., Dlugokencky, E. J. and Bousquet, P.: Methane on the Rise--Again, Science, 343, 493–495, doi:10.1126/science.1247828, 2014.

Oh, Y., Stackhouse, B., Lau, M. C. Y., Xu, X., Trugman, A. T., Moch, J., Onstott, T. C., Jørgensen, C. J., Ludovica, D., Elberling, B., Emmerton, C. A., St. Louis, V. L. and Medvigy, D.: A scalable model explaining methane consumption in arctic mineral soils, Geophys. Res. Lett., 43, 5143–5150, doi:10.1002/2016GL069049, 2016.

Park, R. J., Jacob, D. J., Field, B. D., Yantosca, R. M., and Chin, M.: Natural and transboundary pollution influences on sulfate-nitrate-ammonium aerosols in the United States: Implications for policy, J. Geophys. Res., 109, D15204, doi:10.1029/2003JD004473, 2004.

Parker, R., Boesch, H., Cogan, A., Fraser, A., Feng, L., Palmer, P. I., Messerschmidt, J., Deutscher, N., Griffith, D. W. T., Notholt, J., Wennberg, P. O., and Wunch, D.: Methane observations from the Greenhouse Gases Observing SATellite: Comparison to ground-based TCCON data and model calculations, Geophys. Res. Lett., 38, L15807, doi:10.1029/2011GL047871, 2011.

Peng, S. S., Piao, S. L., Bousquet, P., Ciais, P., Li, B. G., Lin, X., Tao, S., Wang, Z. P., Zhang, Y., and Zhou, F.: Inventory of anthropogenic methane emissions in Mainland China from 1980 to 2010, Atmos. Chem. Phys. Discuss., doi:10.5194/acp-2016-139, in review, 2016.

Pickett-Heaps, C. A., Jacob, D. J., Wecht, K. J., Kort, E. A., Wofsy, S. C., Diskin, G. S., Worthy, D. E. J., Kaplan, J. O., Bey, I., and Drevet, J.: Magnitude of seasonality of wetland methane

emissions from the Hudson Bay Lowlands (Canada), Atmos. Chem. Phys., 11, 3773–3779, doi:10.5194/acp-11-3773-2011, 2011.

Prather, M. J., Holmes, C. D., and Hsu, J.: Reactive greenhouse gas scenarios: systematic exploration of uncertainties and the role of atmospheric chemistry, Geophys. Res. Lett., 39, L09803, doi:10.1029/2012gl051440, 2012.

Rigby, M., Prinn, R. G., Fraser, P. J., Simmonds, P. G., Langenfelds, R. L., Huang, J., Cunnold, D. M., Steele, L. P., Krummel, P. B., Weiss, R. F., O'Doherty, S., Salameh, P. K., Wang, H. J., Harth, C. M., Mühle, J. and Porter, L. W.: Renewed growth of atmospheric methane, Geophys. Res. Lett., 35, L22805, doi:10.1029/2008GL036037, 2008.

Rodgers, C. D.: Inverse Methods for Atmospheric Sounding: Theory and Practice, Vol. 2, edited by: Rodgers, C. D., World Scientific Publishing Co. Pte. Ltd., Singapore, 2000.

Saarnio, S., Winiwarter, W. and Leitão, J.: Methane release from wetlands and watercourses in Europe, Atmos. Environ., 43, 1421–1429, doi:10.1016/j.atmosenv.2008.04.007, 2009.

Sasakawa, M., Machida, T., Tsuda, N., Arshinov, M., Davydov, D., Fofonov, A. and Krasnov, O.: Aircraft and tower measurements of CO_2 concentration in the planetary boundary layer and the lower free troposphere over southern taiga in West Siberia: Long-term records from 2002 to 2011, J. Geophys. Res., 118, 9489–9498, doi:10.1002/jgrd.50755, 2013.

Schubert, C. J., Diem, T. and Eugster, W.: Methane Emissions from a Small Wind Shielded Lake Determined by Eddy Covariance, Flux Chambers, Anchored Funnels, and Boundary Model Calculations: A Comparison, Environ. Sci. Technol., 46, 4515–4522, 2012.

855 Schuur, E. A. G., McGuire, A. D., Schädel, C., Grosse, G., Harden, J. W., Hayes, D. J., Hugelius,
856 G., Koven, C. D., Kuhry, P., Lawrence, D. M., M.Natali, S., Olefeldt, D., Romanovsky, V. E.,
857 Schaefer, K., Turetsky, M. R., Treat, C. C. and Vonk, E. J.: Climate change and the permafrost
858 carbon feedback, Nature, 520, 171–179, doi:10.1038/nature14338, 2015.

859 Shindell, D. T., Faluvegi, G., Koch, D. M., Schmidt, G. A., Unger, N., and Bauer, S. E.:
860 Improved attribution of climate forcing to emissions, Science, 326, 716-718, 2009.

861 Simpson, I. J., Sulbaek Andersen, M. P., Meinardi, S., Bruhwiler, L., Blake, N. J., Helmig, D.,
862 Rowland, F. S. and Blake, D. R.: Long-term decline of global atmospheric ethane concentrations
863 and implications for methane, Nature, 488, 490–494, doi:10.1038/nature11342, 2012.

864 Singh, K., Jardak, M., Sandu, A., Bowman, K., Lee, M., and Jones, D.: Construction of non-
865 diagonal background error covariance matrices for global chemical data assimilation, Geosci.
866 Model Dev., 4, 299-316, 2011.

867 Sweeney, C., Karion, A., Wolter, S., Newberger, T., Guenther, D., Higgs, J. A., Andrews, A. E.,
868 Lang, P. M., Neff, D., Dlugokencky, E., Miller, J. B., Montzka, S. A., Miller, B. R., Masarie, K.
869 A., Biraud, S. A., Novelli, P. C., Crotwell, M., Crotwell, A. M., Thoning, K. and Tans, P. P.:
870 Seasonal climatology of CO_2 across North America from aircraft measurements in the
871 NOAA/ESRL Global Greenhouse Gas Reference Network, J. Geophys. Res. Atmos., 120, 5155–
872 5190, doi:10.1002/2014JD022591, 2015.

873 Tan, Z., Zhuang, Q. and Walter Anthony, K.: Modeling methane emissions from arctic lakes:
874 Model development and site-level study, J. Adv. Model. Earth Syst., 7, 459-483,
875 doi:10.1002/2014MS000314, 2015.

876 Tan, Z. and Zhuang, Q.: Arctic lakes are continuous methane sources to the atmosphere under
877 warming conditions, Environ. Res. Lett., 10, 054016, doi:10.1088/1748-9326/10/5/054016,
878 2015a.

879 Tan, Z. and Zhuang, Q.: Methane emissions from pan-Arctic lakes during the 21st century: An
880 analysis with process-based models of lake evolution and biogeochemistry, J. Geophys. Res.
881 Biogeosciences, 120, 2641–2653, doi:10.1002/2015JG003184, 2015b.

882 Tarnocai, C., Canadell, J. G., Schuur, E. A. G., Kuhry, P., Mazhitova, G. and Zimov, S.: Soil
883 organic carbon pools in the northern circumpolar permafrost region, Global Biogeochem. Cycles,
884 23, GB2023, doi: 10.1029/2008GB003327, 2009.

885 Thompson, R. L., Stohl, A., Zhou, L. X., Dlugokencky, E., Fukuyama, Y., Tohjima, Y., Kim, S.-
886 Y., Lee, H., Nisbet, E. G., Fisher, R. E., Lowry, D., Weiss, R. F., Prinn, R. G., O'Doherty, S.,
887 Young, D. and White, J. W. C.: Methane emissions in East Asia for 2000 – 2011 estimated using
888 atmospheric Bayesian inversion, J. Geophys. Res. Atmos., 120, 4352–4369,
889 doi:10.1002/2014JD022394, 2015.

890 Thornton, B. F., Geibel, M. C., Crill, P. M., Humborg, C. and Mörth, C.-M.: Methane fluxes
891 from the sea to the atmosphere across the Siberian shelf seas, Geophys. Res. Lett., 43, 5869–
892 5877, doi:10.1002/2016GL068977, 2016.

893 Turner, A. J., Jacob, D. J., Wecht, K. J., Maasakkers, J. D., Biraud, S. C., Boesch, H., Bowman,
894 K. W., Deutscher, N. M., Dubey, M. K., Griffith, D. W. T., Hase, F., Kuze, A., Notholt, J.,
895 Ohyama, H., Parker, R., Payne, V. H., Sussmann, R., Velazco, V. A., Warneke, T., Wennberg, P.
896 O. and Wunch, D.: Estimating global and North American methane emissions with high spatial

resolution using GOSAT satellite data, Atmos. Chem. Phys., 15, 7049–7069, doi:10.5194/acp-15-7049-2015, 2015.

van der Werf, G. R., Randerson, J. T., Giglio, L., Collatz, G. J., Mu, M., Kasibhatla, P. S., Morton, D. C., DeFries, R. S., Jin, Y., and van Leeuwen, T. T.: Global fire emissions and the contribution of deforestation, savanna, forest, agricultural, and peat fires (1997–2009), Atmos. Chem. Phys., 10, 11,707–11,735, doi:10.5194/acp-10-11707-2010, 2010.

Walter, K. M., Zimov, S. A., Chanton, J. P., Verbyla, D. and Chapin III, F. S.: Methane bubbling from Siberian thaw lakes as a positive feedback to climate warming, Nature, 443, 71–75, doi:10.1038/nature05040, 2006.

Walter, K. M., Smith, L. C. and Chapin III, F. S.: Methane bubbling from northern lakes: present and future contributions to the global methane budget, Philos. T. Roy. Soc. A, 365(1856), 1657–76, doi:10.1098/rsta.2007.2036, 2007.

Wania, R., Melton, J. R., Hodson, E. L., Poulter, B., Ringeval, B., Spahni, R., Bohn, T., Avis, C. A., Chen, G., Eliseev, A. V., Hopcroft, P. O., Riley, W. J., Subin, Z. M., Tian, H., van Bodegom, P. M., Kleinen, T., Yu, Z. C., Singarayer, J. S., Zürcher, S., Lettenmaier, D. P., Beerling, D. J., Denisov, S. N., Prigent, C., Papa, F. and Kaplan, J. O.: Present state of global wetland extent and wetland methane modelling: methodology of a model inter-comparison project (WETCHIMP), Geosci. Model Dev., 6, 617–641, doi:10.5194/gmd-6-617-2013, 2013.

Wang, J. S., Logan, J. L., McElroy, M. B., Duncan, B. N., Megretskaia, I. A., and Yantosca, R. M.: 3-D model analysis of the slowdown and interannual variability in the methane growth rate from 1988 to 1997, Global Biogeochem. Cycles, 18, GB3011, doi:10.1029/2003GB002180, 2004.

Wecht, K. J., Jacob, D. J., Frankenberg, C., Jiang, Z. and Blake, D. R.: Mapping of North American methane emissions with high spatial resolution by inversion of SCIAMACHY satellite data, J. Geophys. Res. Atmos., 119, 7741–7756, doi:10.1002/2014JD021551, 2014.

Zhu, X., Zhuang, Q., Qin, Z., Glagolev, M. and Song, L.: Estimating wetland methane emissions from the northern high latitudes from 1990 to 2009 using artificial neural networks, Global Biogeochem. Cycles, 27, 1–13, doi:10.1002/gbc.20052, 2013.

Zhuang, Q., Melillo, J. M., Kicklighter, D. W., Prinn, R. G., McGuire, A. D., Steudler, P. A., Felzer, B. S., and Hu, S.: Methane fluxes between terrestrial ecosystems and the atmosphere at northern high latitudes during the past century: A retrospective analysis with a process-based biogeochemistry model, Global Biogeochem. Cycles, 18, GB3010, doi:10.1029/2004GB002239, 2004.

Zhuang, Q., Melillo, J. M., Sarofim, M. C., Kicklighter, D. W., McGuire, a. D., Felzer, B. S., Sokolov, A., Prinn, R. G., Steudler, P. a. and Hu, S.: CO_2 and CH_4 exchanges between land ecosystems and the atmosphere in northern high latitudes over the 21st century, Geophys. Res. Lett., 33, L17403, doi:10.1029/2006GL026972, 2006.

Zhuang, Q., Melillo, J. M., McGuire, A. D., Kicklighter, D. W., Prinn, R. G., Steudler, P. A., Felzer, B. S. and Hu, S.: Net emissions of CH_4 and CO_2 in Alaska: Implications for the region's greenhouse gas budget, Ecol. Appl., 17, 203–212, 2007.

940 Figure Captions

941 Figure 1. SCIAMACHY retrievals (n = 37743) of the weighted column-average CH_4 dry mole
942 fractions for July 2005–September 2005 in the pan-Arctic that have passed all quality control
943 tests described in Section 2.1 and the locations of surface flask stations and aircraft missions
944 used for data assimilation or inversion evaluation.

945 Figure 2. Prior average CH_4 fluxes from wetlands, lakes and other sources (i.e. anthropogenic
946 and biomass burning) in 2005 used for the pan-Arctic nested grid inversions at 1/2° × 2/3°
947 resolution. Annual total emission for each pan-Arctic source is presented in units of Tg CH_4 yr^{-1}.

948 Figure 3. Bias correction function (left) and standard deviation (right) for SCIAMACHY
949 retrievals overpassing the pan-Arctic. ΔXCH_4 is the difference between SCIAMACHY and
950 column-average mixing ratios mapped from aircraft vertical profiles. The red line in the left
951 shows a linear regression weighted by the number of SCIAMACHY retrievals.

952 Figure 4. Optimized pan-Arctic CH_4 fluxes in 2005 at 1/2° × 2/3° resolution using both
953 SCIAMACHY and NOAA/ESRL observations. a) BERN; b) CLM4Me; c) DLEM; d)
954 ORCHIDEE; e) SDGVM; f) WSL.

955 Figure 5. Comparison of prior and posterior pan-Arctic CH_4 emissions and their uncertainties.
956 "NOAA only" represents posterior emissions assimilating only surface measurements. "NOAA +
957 SCIA" represents posterior emissions assimilating both surface measurements and satellite
958 retrievals. The uncertainty of prior emissions is 100%. Scenarios are represented by their name
959 initials: "B" for BERN, "C" for CLM4Me, "D" for DLEM, "O" for ORCHIDEE, "S" for
960 SDGVM and "W" for WSL.

961 Figure 6. Distribution of the relative difference between the observed and simulated posterior
962 SCIAMACHY column-average mixing ratios. The "DLEM + Lake" scenario includes CH_4
963 emissions from both wetlands and lakes and the "DLEM only" scenario only includes CH_4
964 emissions from wetlands. Relative difference is calculated as a percentage of absolute
965 differences between GEOS-Chem and SCIAMACHY relative to SCIAMACHY retrievals. Two
966 extending red and blue lines represent the means of the simulation bias under the "DLEM + Lake"
967 scenario and the "DLEM only" scenario, respectively.

968 Figure 7. Evaluation of the posterior GEOS-Chem CH_4 mole fractions from the pan-Arctic
969 nested-grid inversions with independent data sets from the NOAA flask stations, the NOAA
970 aircraft PFA profiles and the NIES aircraft Surgut profiles. Black symbols indicate the rms of the
971 forward GEOS-Chem runs and red symbols indicate the rms of the global inversions.

Table1. Summary of bias correction methods and of mean absolute satellite-model difference (ppb) for 2003-2005 before and after applying bias correction. ΔBIC is the BIC score increase of a bias correction method when referring to the latitude only method.

	Bias correction function*	Mean absolute difference	ΔBIC	R^2
No correction		9.271		
Latitude only	$p_0 + p_1\varphi + p_2\varphi^2$	6.305		0.62
Air mass factor only	$p_0 + p_1 A_F$	7.071	161	0.52
Humidity only	$p_0 + p_1 H_S$	6.786	73	0.56
Latitude + Humidity	$p_0 + p_{11}\varphi + p_{12}\varphi^2 + p_{21} H_S$	6.230	-7	0.62
Air mass factor + Humidity	$p_0 + p_{11} A_F + p_{21} H_S$	6.396	12	0.60

* p_0, p_1, p_2, p_{11}, p_{12} and p_{21} are regression parameters.

Table 2. Estimated annual CH_4 emissions (units: Tg CH_4 yr^{-1}) for TransCom 3 land regions (NAB: North American Boreal, NAT: North American Temperate, SATr: South American Tropical, SAT: South American Temperate, NAf: Northern Africa, SAf: Southern Africa, ErB: Eurasian Boreal, ErT: Eurasian Temperate, TrA: Tropical Asia, Aus: Australasia, and Eur: Europe). The priors are the range of the initial CH_4 emissions given by the six scenarios.

Region	**Priors**	**Posterior**						**Fraser et al. (2013)**	**Alexe et al. (2015)**
		Bern	**CLM4Me**	**DLEM**	**ORCHIDEE**	**SDGVM**	**WSL**		
NAB	7.9–26.0	24.3	16.2	16.8	27.4	12.0	20.7	5.1±1.1	10.3
NAT	38.5–59.2	33.2	32.8	42.8	49.2	51.2	39.7	62.5±4.4	45.6
SATr	29.6–100.0	43.0	60.8	31.4	61.0	62.3	42.1	49.6±6.4	71.8
SAT	29.1–55.8	31.2	27.1	35.2	39.1	25.6	30.5	55.8±9.5	40.2
NAf	26.8–31.2	34.0	41.3	27.9	28.0	27.7	32.0	46.9±7.3	50.6
SAf	16.0–27.0	18.4	16.2	19.0	24.2	15.6	18.7	36.6±5.8	42.0
ErB	11.5–32.7	19.2	14.3	16.5	18.7	22.2	14.9	16.5±3.8	15.4
ErT	114.9–133.5	97.0	84.9	146.1	92.7	98.3	99.8	115.9±7.3	109.6
TrA	33.1–45.8	47.3	51.4	35.8	33.1	36.4	45.1	43.5±3.2	76.8
Aus	5.8–8.3	7.3	7.7	6.6	7.9	6.3	7.3	17.6±2.7	4.3
Eur	43.6–53.5	54.9	52.2	46.4	43.5	56.5	54.1	39.6±3.7	28.9
Wetlands	121.7–278.1	166.8	164.6	130.0	203.3	161.8	160.7	192.1±16.1	169
Global	471.5–627.8	501.0	497.7	511.5	511.0	496.4	502.9	510.6±18.4	540.5

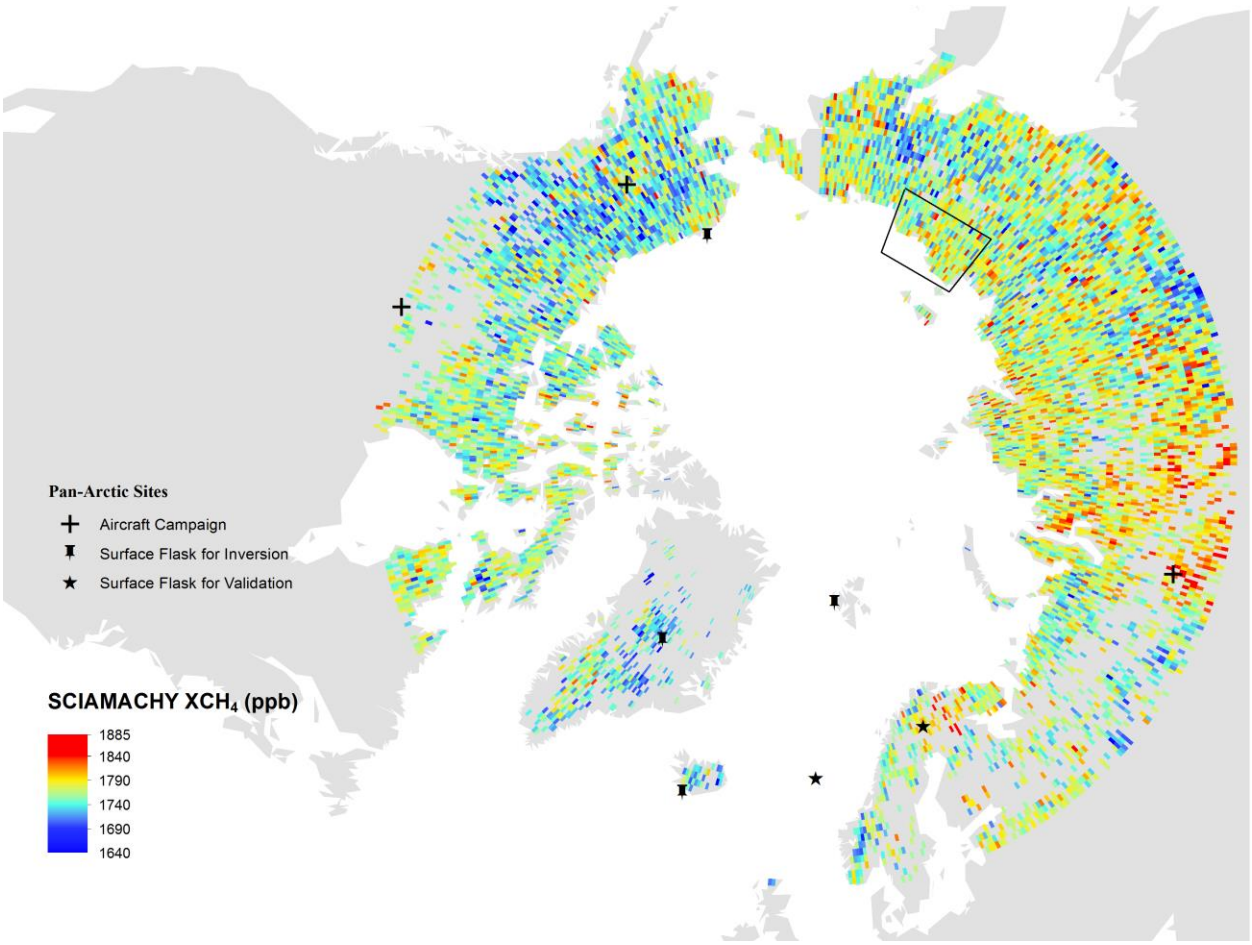
Pan-Arctic Sites
Aircraft Campaign
Surface Flask for Inversion
Surface Flask for Validation
SCIAMACHY XCH4 (ppb)
1885
1840
1790
1740
1690
1640

Figure 1.

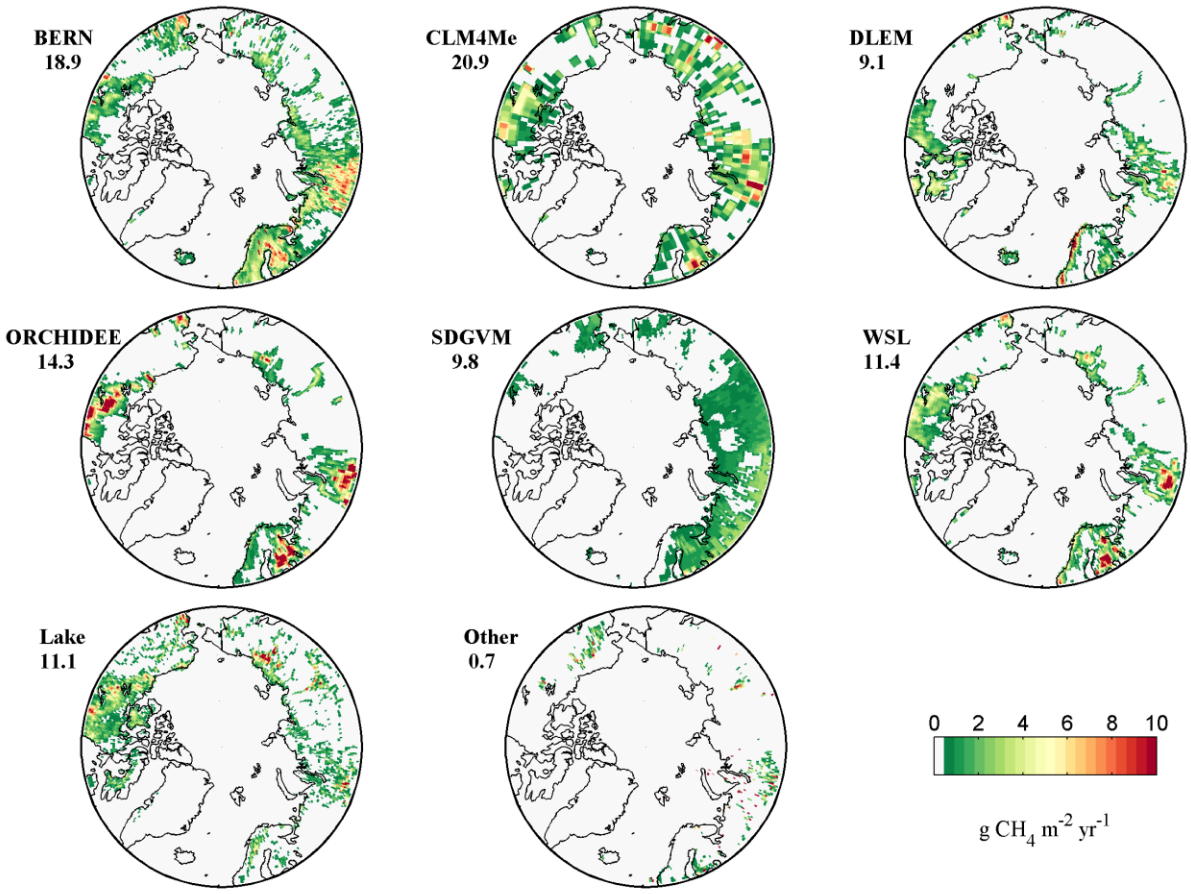
BERN
18.9
CLM4Me
20.9
DLEM
9.1
ORCHIDEE
14.3
SDGVM
9.8
WSL
11.4
Lake
11.1
Other
0.7
0 2 4 6 8 10
g CH4 m-2 yr-1

Figure 2.

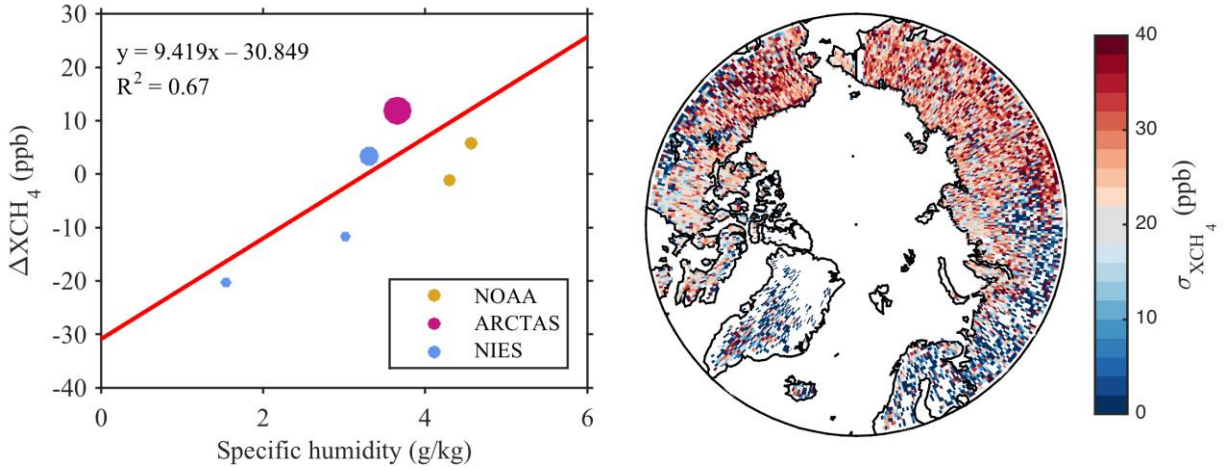
y = 9.419x – 30.849
R2 = 0.67
ΔXCH4 (ppb)
Specific humidity (g/kg)
NOAA
ARCTAS
NIES
σXCH4 (ppb)

Figure 3.

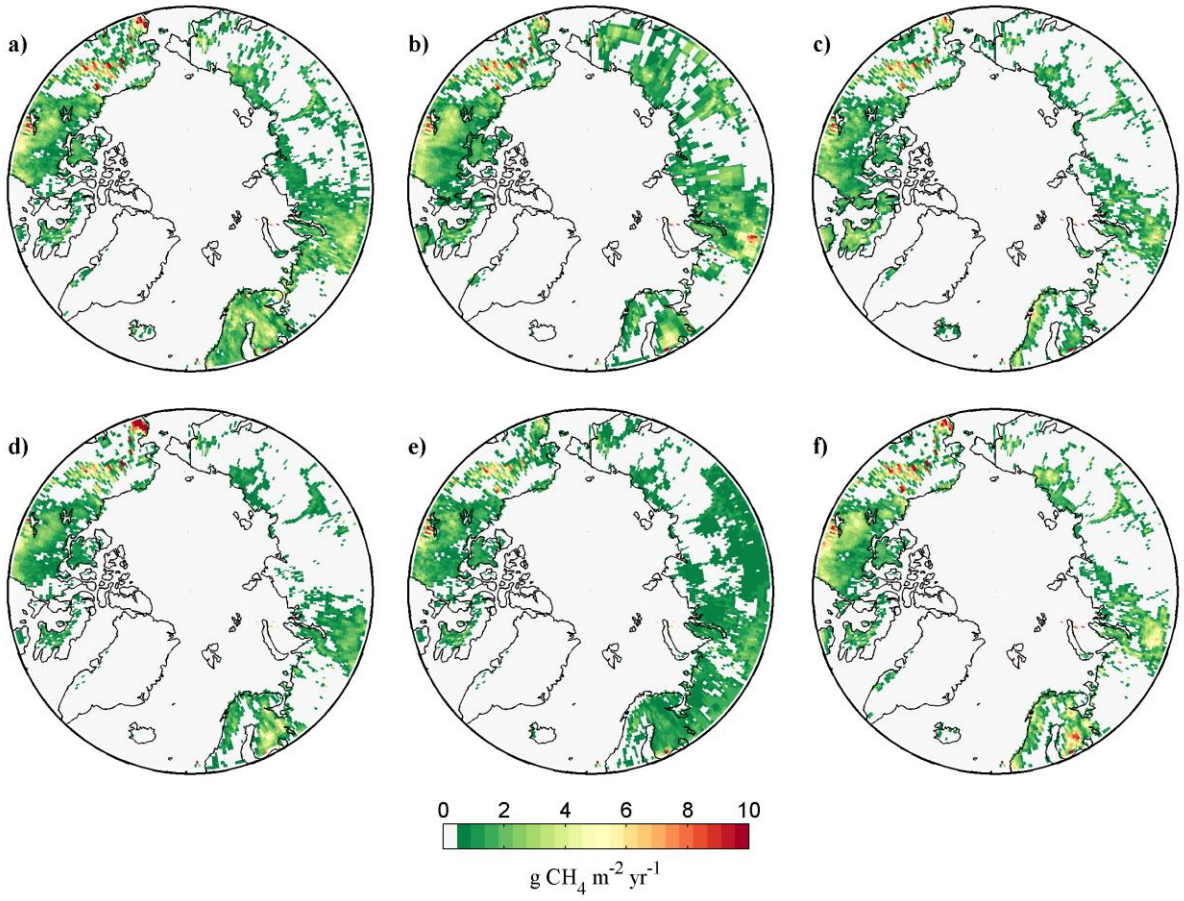

Figure 4.

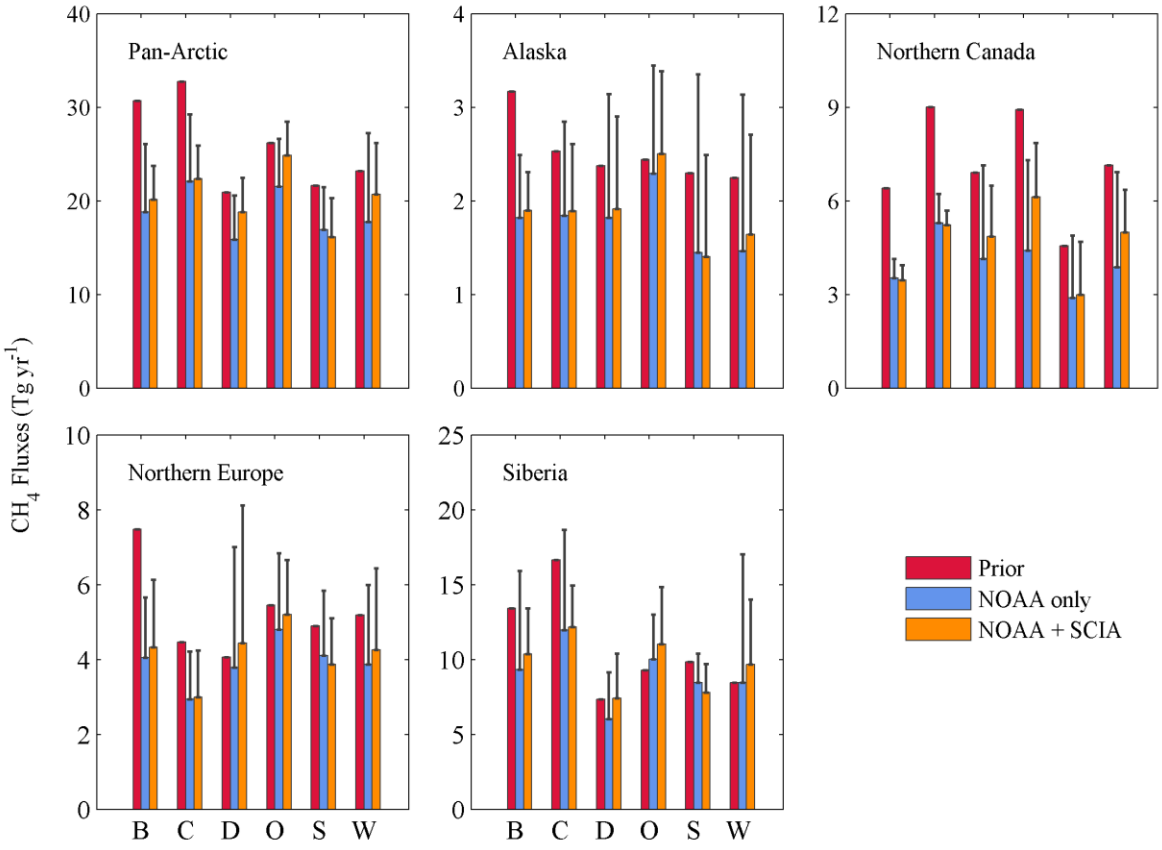
Pan-Arctic
Alaska
Northern Canada
Northern Europe
Siberia
CH4 Fluxes (Tg yr-1)
B C D O S W
Prior
NOAA only
NOAA + SCIA

Figure 5.

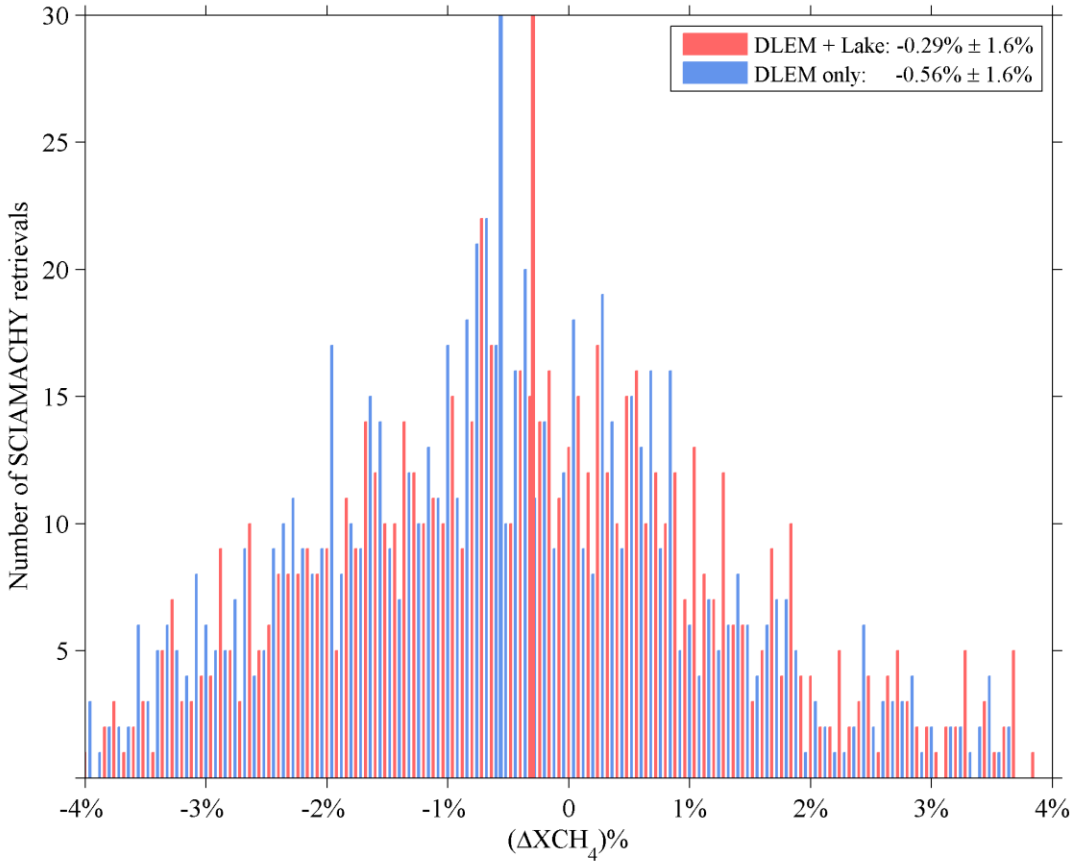
DLEM + Lake: -0.29% ± 1.6%
DLEM only: -0.56% ± 1.6%
Number of SCIAMACHY retrievals
30
25
20
15
10
5
-4%
-3%
-2%
-1%
0
1%
2%
3%
4%
(ΔXCH4)%

Figure 6.

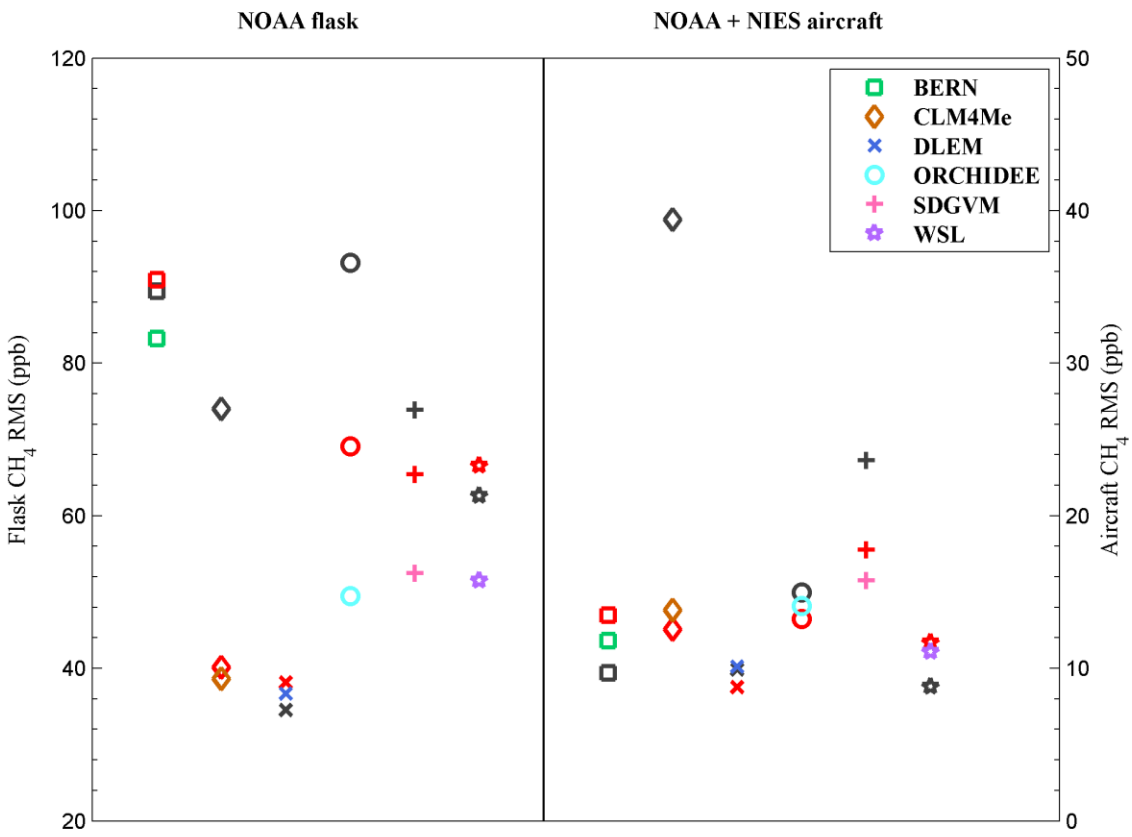
NOAA flask
NOAA + NIES aircraft
Flask CH4 RMS (ppb)
Aircraft CH4 RMS (ppb)
120
100
80
60
40
20
50
40
30
20
10
0
BERN
CLM4Me
DLEM
ORCHIDEE
SDGVM
WSL

Figure 7.